

Contract Research Division
NATIONAL RESEARCH CORPORATION
70 Memorial Drive
Cambridge, Massachusetts 02142

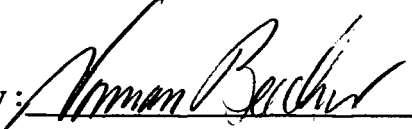
FINAL REPORT
DEVELOPMENT OF A
MASS SPECTROMETER DESIGN

P. Blum
F. L. Torney, Jr.

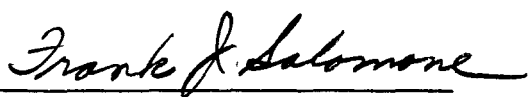
June 1, 1964 - December 31, 1964
NAS1-2691-6

March 23, 1965

Approved by:


Norman Beecher
Assistant Director
of Research

Reviewed by:


Frank J. Salomone
Contracts Manager

Submitted to:

National Aeronautics and Space Administration
Langley Research Center
Langley Station
Hampton, Virginia

Attention:

Mr. Leon W. Fitchett, Contracting Officer

Abstract

This report covers the second phase of a four phase program to develop a cold cathode ion source mated to a quadrupole mass spectrometer. The completed unit is to be used as a residual gas analyzer. The cold cathode (magnetron) ion source was chosen because of lower background noise and higher sensitivities than the usual hot-filament types. This report describes the design of the ion source and the mass spectrometer and gives details of the construction and experiments with the ion source.

TABLE OF CONTENTS

	<u>Page #</u>
LIST OF ILLUSTRATIONS	ii
OBJECTIVE	iv
INTRODUCTION	1
I ION SOURCE DESIGN	3
A. Overall Electrical and Mechanical Design	3
B. The Magnetron	8
C. The Probe	9
D. The Lens	10
1. Analytical approach, lens limitations	10
2. Design and operation	14
II EXPERIMENTAL PROCEDURES AND AUXILIARY APPARATUS	18
III EXPERIMENTAL RESULTS AND CONCLUSIONS	24
A. Ion Beam Studies Without the Lens	24
1. Ion energy distribution vs V_{K1}	24
2. Ion energy distribution vs distance	29
B. Lens Effectiveness	35
C. Vacuum Performance Characteristics	45
IV QUADRUPOLE MASS SPECTROMETER DESIGN	46
A. Summary of Design Criteria	46
B. Design Chart	49
1. Construction	49
2. Interpretation & selection of values	51
SUMMARY AND CONCLUSIONS	55
BIBLIOGRAPHY	59

LIST OF ILLUSTRATIONS

Page #

FIG. 1	COLD CATHODE ION SOURCE WITH LENS (ELECTRICAL SCHEMATIC)	4
FIG. 2	COLD CATHODE ION SOURCE (APPROX. FULL SIZE)	5
FIG. 3	VIEW OF INTERNAL COMPONENTS OF COLD CATHODE ION SOURCE. FROM TOP TO BOTTOM: MAGNETRON, LENS & PROBE	6
FIG. 4	GRAPH FOR DETERMINING FOCAL LENGTHS (FROM ZWORYKIN ¹¹)	16
FIG. 5	VACUUM SYSTEM SCHEMATIC	20
FIG. 6	VIEW OF THE UPPER MANIFOLD PORTION OF THE VACUUM SYSTEM	21
FIG. 7	VIEW OF VACUUM SYSTEM AND ASSOCIATED ELECTRONICS	22
FIG. 8	COLLECTOR CURRENT VS COLLECTOR POTENTIAL FOR SELECTED PUSHER CATHODE POTENTIALS (V_{K1})	25
FIG. 9	DIFFERENTIAL COLLECTOR CURRENT VS PUSHER CATHODE POTENTIAL FOR SELECTED INTERVALS OF COLLECTOR POTENTIAL	28
FIG. 10	SENSITIVITY VS INTEGRAL ION ENERGY AT 0.61 INCHES, FOR V_{K1} AT +40 VOLTS	30
FIG. 11	DIFFERENTIAL COLLECTOR CURRENT VS DISTANCE FOR SELECTED ENERGY INTERVALS, FOR $V_{K1} = +40$ VOLTS	31
FIG. 12	DIFFERENTIAL COLLECTOR CURRENT VS DISTANCE FOR SELECTED ENERGY INTERVALS, FOR $V_{K1} = \text{ZERO}$ VOLTS	32
FIG. 13	DIFFERENTIAL COLLECTOR CURRENT VS DISTANCE FOR SELECTED ENERGY INTERVALS, FOR $V_{K1} = -40$ VOLTS	33

LIST OF ILLUSTRATIONS (Cont'd)

	<u>Page #</u>
FIG. 14 EFFECT OF LENS POTENTIAL VARIATIONS: I _c VS V _{L2} FOR SELECTED V _c VALUES AT POSITION 1, V _{K1} = ZERO VOLTS	37
FIG. 15 EFFECT OF LENS POTENTIAL VARIATIONS: I _c VS V _{L2} FOR SELECTED V _c VALUES AT POSITION 1, V _{K1} = +40 VOLTS	38
FIG. 16 EFFECT OF LENS POTENTIAL VARIATIONS: I _c VS V _{L2} FOR SELECTED V _c VALUES AT POSITION 2, V _{K1} = ZERO VOLTS	40
FIG. 17 EFFECT OF LENS POTENTIAL VARIATIONS ON I _c AND I _Q AT POSITION 2 FOR V _{K1} = ZERO VOLTS	42
FIG. 18 EFFECT OF LENS POTENTIAL VARIATIONS ON I _c AND I _Q AT POSITION 3, FOR V _{K1} = +40, ZERO AND -40 VOLTS	43
FIG. 19 ION AND ELECTRON ENERGY SPECTRA AT FOCUSING POTENTIAL FOR POSITION 3: V _{L2} = +420 VOLTS	44
FIG. 20 SCHEMATIC OF QUADRUPOLE MASS ANALYZER	47
FIG. 21 QUADRUPOLE MASS ANALYZER DESIGN CHART	52

OBJECTIVE

The objective of this program has been to develop and test an improved cold cathode ion source for use with a quadrupole mass analyzer. The primary aim has been to increase the sensitivity of the source consistent with the requirements of a practical analyzer, of which a preliminary design has been made.

INTRODUCTION

This program has been undertaken to fill the need for a mass spectrometer for measuring partial pressures in the ultrahigh vacuum (UHV) and extreme high vacuum (XHV) regions. Two fundamental problems have limited this capability in the past, both lying with the ion source portion of the spectrometer. One is insufficient source sensitivity. The other pertains to source cleanliness.

Mass spectrometers commonly use an ion source with a hot filament, the latter supplying electrons in abundance for molecular ionization. While this type of device has much to recommend it, the above stated problems severely restrict its usefulness in ultrahigh vacuum. A primary difficulty is that the heat generated causes both decomposition of gases and their evolution from the source itself, thus causing confusion in both the type and amount of gases to be measured. Cold cathode ion gauges of the magnetron type^(1,2) on the other hand have sharply reduced this difficulty while producing the highest sensitivities thus far attained; the sensitivity of these devices results from immensely increased electron path lengths, effected by crossed electric and magnetic fields. This research program has been directed toward adapting a cold cathode magnetron type discharge for use with a mass analyzer.

The first phase of this program (Contract NAS1-2691, Task 2)⁽³⁾, demonstrated the feasibility of this approach by constructing and

testing a cold cathode ion source. In essence, the source consisted of a magnetron configuration modified to allow extraction of the ions from the discharge. The ions are thus accessible for analysis with a mass spectrometer. Studies revealed, among other salient characteristics, an ion beam sensitivity of 5 ma/torr after passing through an aperture 3.0 mm in diameter. This is 500 times the sensitivity of conventional hot filament mass spectrometer ion sources. A companion study showed that a quadrupole mass spectrometer was best suited to the energy and dimensions of this beam and tentative design parameters were specified.

The present phase of the program has been directed toward developing and testing an improved source design. In particular, methods are investigated for improving beam intensity compatible with the energy and dimensional requirements of a quadrupole mass analyzer. A quadrupole design chart has been composed to aid in optimally matching source and quadrupole characteristics.

The new source has been designed to include some improvements while deferring others to allow versatility in determining optimum electronic parameter values, optimum positioning between source and quadrupole and to allow testing the effectiveness of an electrostatic lens. Source and experiments were designed for study of source response to variations in pressure and gas composition subsequent to optimization studies.

I ION SOURCE DESIGN

A. Overall Electrical and Mechanical Design

Figure 1 and Figure 2 illustrate, respectively, the electrical schematic of the source and the more detailed mechanical layout, drawn approximately to scale. Figure 3 is a photograph of the internal components mounted on the flange.

Three sections are shown as follows:

1. The magnetron portion or source proper. This consists of a pusher cathode (K_1), an extractor cathode (K_2), an anode (A), two auxiliary cathodes and a stack of five (5) cylindrical magnets.
2. An electrostatic lens. This consists of three aperture plates L_1 , L_2 and L_3 .
3. A probe. This consists of a simulated quadrupole aperture plate (Q) and a Faraday cup or ion collector (C). It is used for studying ion beam characteristics and can be made to simulate the dimensional and energy restrictions of a quadrupole mass analyzer.

The source has been designed so that both probe and lens are moveable with respect to the magnetron and each other and so that experiments may be conducted with the lens either in or out of the system. Electronic access has been provided to allow monitoring currents and/or applying potentials to K_1 , A, L_2 , Q and C.

Each of the three sections are supported on a steel mounting cylinder either by direct spot welding or via insulated spacers (sapphire balls are used for L_2 and the anode, kovar-to-glass studs

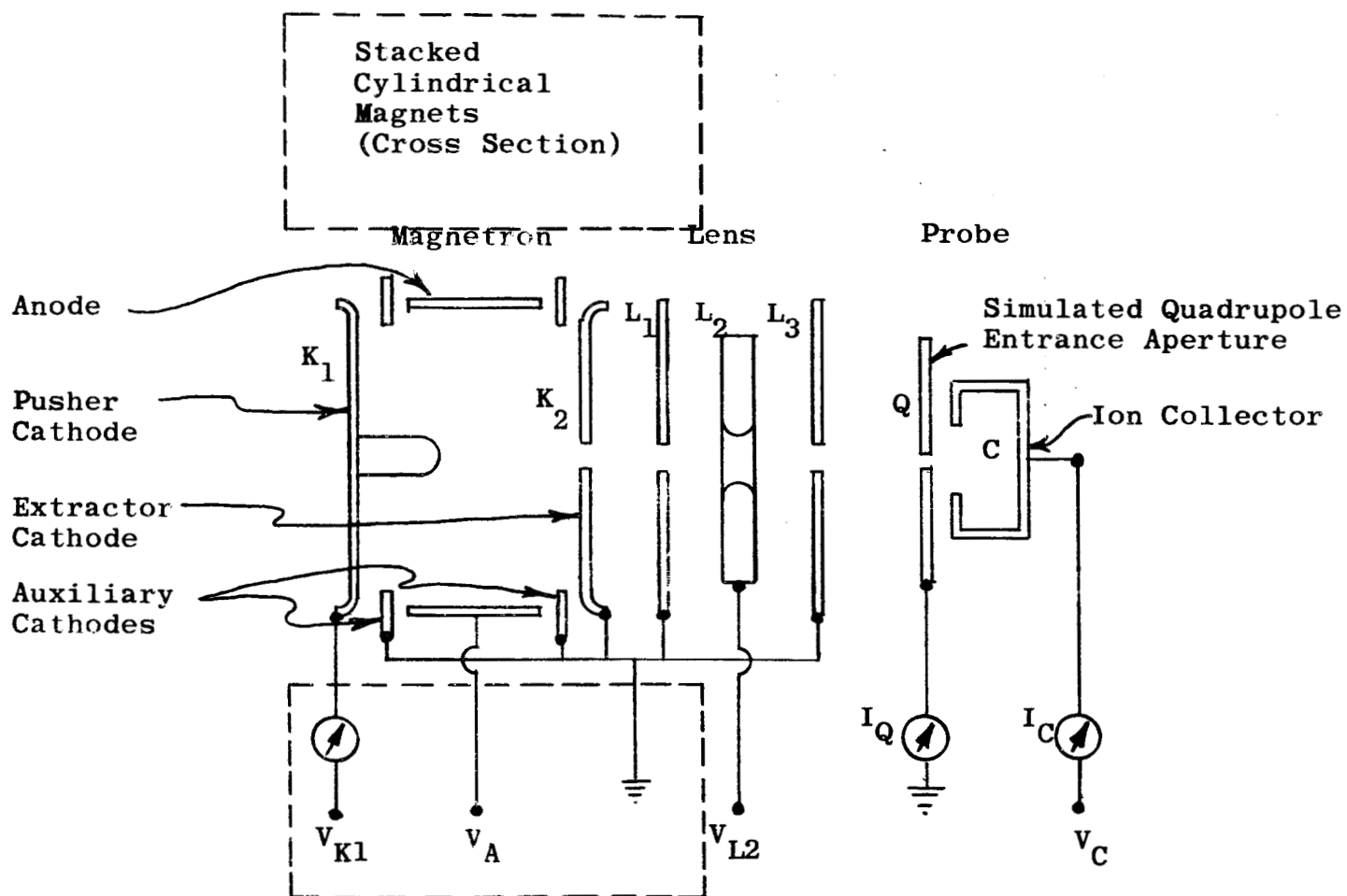


FIG. 1 COLD CATHODE ION SOURCE WITH LENS (ELECTRICAL SCHEMATIC)

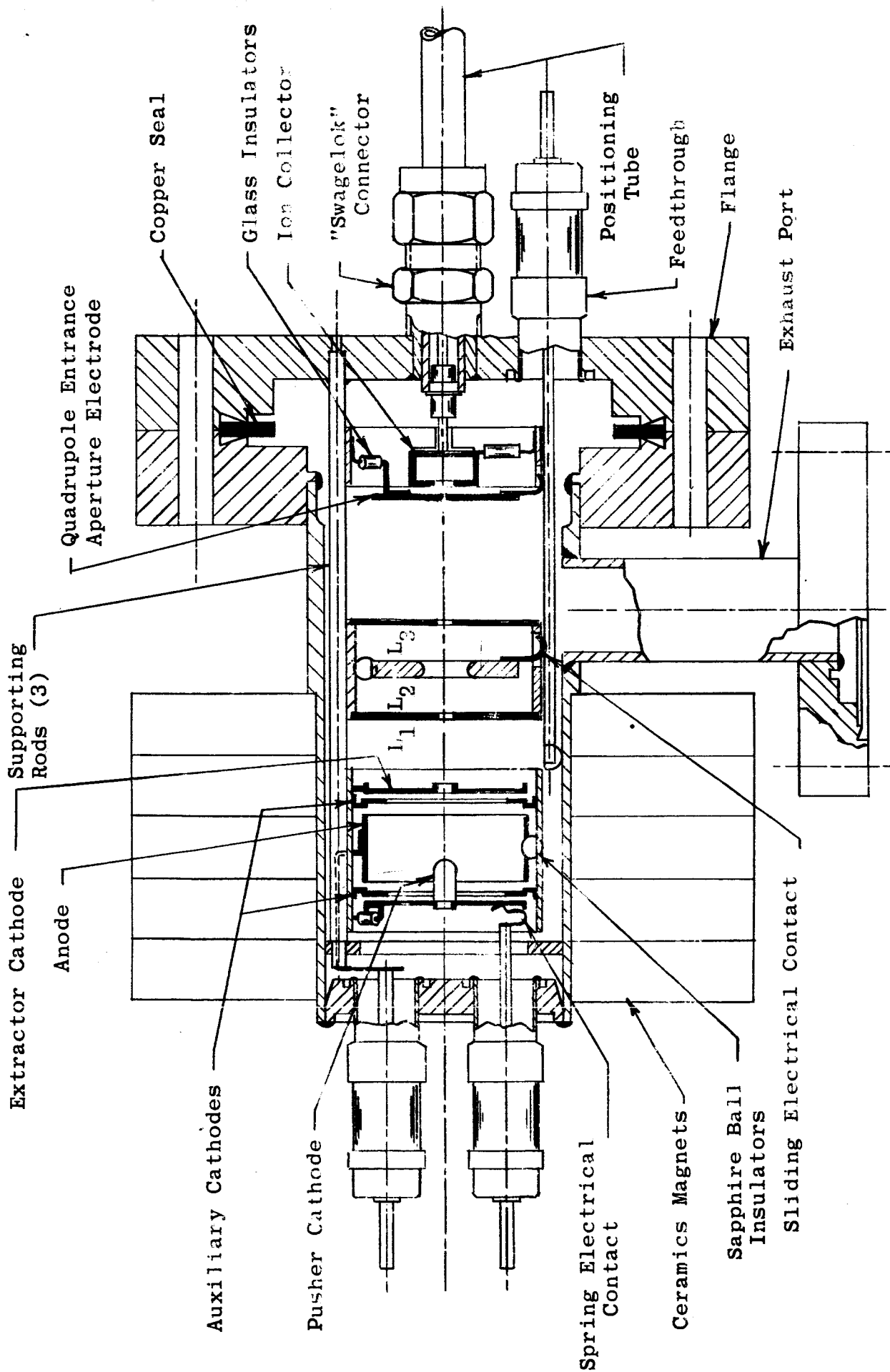


FIG. 2 COLD CATHODE ION SOURCE (APPROX. FULL SIZE)

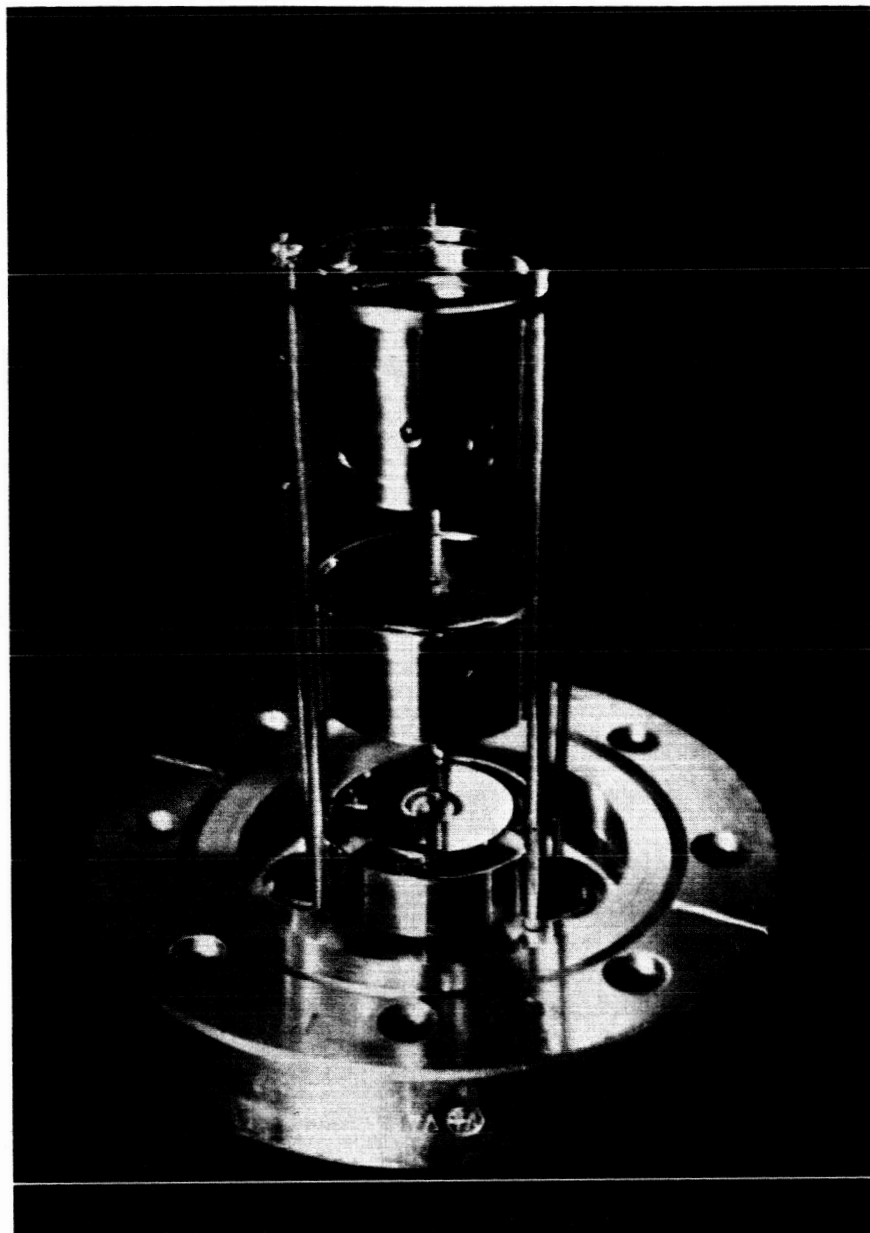


FIG. 3 VIEW OF INTERNAL COMPONENTS OF COLD CATHODE
ION SOURCE. FROM TOP TO BOTTOM:
MAGNETRON, LENS AND PROBE

for the remaining elements). The mounting cylinders are supported on three steel rods which are welded to a flange. Electrically, this design provides a guard-ring arrangement for all elements not operating at ground potential. Mechanically, the design permits alignment and inspection of components when the flange is removed from the housing.

Positioning is accomplished by sliding the lens and/or probe along the three supporting rods. The probe is adjustable with a positioning rod, which passes through a "Swagelok" connector, without opening the flange. The lens assembly is moved forward by pushing with the probe. (The flange must be removed to move the lens backward). Measurements on the positioning rod outside the source enables determination of distances between the lens, magnetron and probe.

The "Swagelok" connector was designed for use during source sensitivity studies only (both with and without the lens), at pressures in the 10^{-8} torr range. Since the "Swagelok's" teflon washers are not bakeable at high temperatures it is essential that they be removed for studies at lower pressures. (The plan originally called for replacement of the entire connector with a ceramic feedthrough welded into the flange subsequent to the sensitivity studies. For reasons discussed in Section IIIC, this plan was not followed. It should also be indicated that the "Swagelok" proved less beneficial than expected due to its tendency to bind.

Feedthroughs are made of a high alumina ceramic, 430 stainless steel and a gold alloy seal. Ion source elements are of Nichrome-V, while the remaining elements and housing are of 303 or 304 stainless steel. All flanges are standard Varian "Conflat" flanges using a copper gasket. The materials used enable the entire unit (with teflon washers removed) to be baked at 450°C. Sealed joints are heli-arc welded. These have been kept internal wherever possible to prevent gas traps.

B. The Magnetron

The magnetron portion of the cold cathode ion source, in both the feasibility study and in the present one, is a modification of the magnetron gauge described by Redhead⁽¹⁾. The reasons underlying its choice over other types of cold cathode discharges can be found in the final report⁽³⁾ of the feasibility study, together with a comprehensive bibliography on the subject. Application of the magnetron gauge as an ion source for spectrometry purposes required that the normal magnetron configuration be modified to allow an extracted ion beam. This was accomplished by separating the single, spool shaped cathode into two cathodes, one with a remnant stub and one with an aperture. Modification of the horseshoe magnet ordinarily used was also necessary.

In the present source the magnetic arrangement was further modified. Magnetic pole pieces which were in front of cathode K_2 and behind cathode K_1 have been removed (Figure 1). In addition,

the array of horseshoe Alnico magnets previously used have been replaced by a stack of cylindrical ceramic magnets. Among the benefits of this modification are the following: (1) Elimination of pole pieces reduces surface area and gas traps to allow improved UHV performance. (2) The quadrupole can be brought closer to the ion exit aperture (K_2) for more efficient utilization of extracted ions - whether a lens is used or not. (3) The cylindrical magnets provide a far more compact design than those previously used.

Provision has been made for monitoring cathode current at K_1 (which indicates total pressure) and for applying a potential drop between K_1 and K_2 to study the effect of this potential on the extraction of low energy ions. Cathode K_2 has been grounded to keep it at the same potential as Q. Since Q must be grounded for proper operation of the quadrupole this arrangement prevents undesirable lens action in the intervening space.

C. The Probe

The probe, shown in Figures 1, 2, and 3, is a commonly used method of exploring ion energy distributions. It consists of a Faraday cup or ion collector C preceded by an aperture plate Q, which serves as an electrostatic shield.

An ion beam incident on Q and C when both are of ground potential will produce a current at C (I_c). This will be produced by ions of all energies incident. However, if a positive potential

is applied to C (V_c), ions with energy less than eV_c , where e is the charge on the ion, will have insufficient energy to overcome the potential barrier and will be turned away. A plot of I_c vs V_c will therefore provide the ion energy distribution of that portion of the beam passing through Q.

By making the aperture in Q to correspond to the dimensional restrictions of a quadrupole mass spectrometer and the retarding potential V_c to correspond to the energy restrictions, the probe serves to give the useable source sensitivity in amps/torr referred to a quadrupole entrance. A Q aperture of 1 mm was used in the present study. The probe was designed to be moveable so that beam characteristics could be measured as a function of distance from the source as well as a function of different object and image distances with the lens in use.

In practice the beam emerging from K_2 contains electrons as well as ions. This serves to make I_c negative when V_c exceeds some positive value. When I_c is plotted against V_c , to obtain the ion energy distribution, special problems of interpretation result which will be discussed with the presentation of experimental results in Section III.

D. The Lens

1. Analytical approach, lens limitations:

Literature on the optics of charged particles is almost totally concerned with electrons. While the laws governing ion and electron optics are essentially identical, the properties of the present

source and the requirements of the present lens pose fundamental differences in the problems of usual concern in electron optics.

The peculiar beam properties of the cold cathode ion source, which must be anticipated, are large divergence, lack of homocentricity and large ion energy spread, (from an optical view point). The peculiar lens requirements are concentration of the largest number of ions from this beam into a small aperture (1 mm in diameter) while maintaining minimum ion energy (for optimum source sensitivity - discussed in Section IV).

An electrostatic lens was chosen for this work over a magnetic one. Among its relative advantages are small bulk, versatility and a focal length independent of charge to mass ratio $(e/m)^{(4)}$. As a result of the latter, electron electrostatic lens studies, including experimentally determined focal lengths, are applicable to the present ion lens design.

The approach taken to the lens design was to treat the quadrupole entrance aperture as image and the ion source extractor aperture as object. Since for every object point there must then be a conjugate image point, it follows, (discounting aberration effects and aperture limitations) that all ions from the object hole must land in the image hole. This approach eliminates the need for knowing the extracted ions' angular distribution and requires no restrictive assumptions, such as beam homocentricity.

To ascertain optimum lens design and optimum operating parameters, a most pertinent fundamental optical relationship, Abbe's sine

law, was enlisted. Derivable from the principle of least action⁽⁵⁾, it is independent of lens system or type of radiation. Applying it to ion optics, a relationship is obtained between image current intensity (current/unit area) and radial and axial ion energy, namely

$$j' = j(V' \sin^2 \theta' / V \sin^2 \theta).$$

Here, j' and j represent ion current intensity at image and object, respectively; θ' and θ represent the angle which arbitrary ion paths make with the lens axis at image and object, respectively; V' and V represent corresponding ion energy per unit charge at the image and object, respectively.

It can be seen that a fundamental limitation is placed upon the maximum attainable image intensity by the ion energy restrictions at the image imposed by a mass analyzer. High image intensity requires large V' and/or large θ' , while low axial and radial energy at the image requires small V' and θ' . An optimum compromise between the two goals is therefore necessary.

Abbe's sine law also provides one of the important reasons for choice of an einzel lens design. Here, ions leaving the lens have the same energy as those entering. It therefore, has been possible to design a lens (discussed in Section ID-2) so that $V'=V$, thus leaving total ion energy intact. This is at the expense of increasing the radial component of the energy. However, the radial component increases only as the square root of the total energy

increase which would be required of an accelerating lens to produce the same intensity.

An additional source of intensity limitation arises because source ions are not monoenergetic. Reduced intensity here results because ions of different energy cannot produce an image at the quadrupole entrance aperture for the same lens operating conditions. Since no methods presently exist for the solution of this problem (chromatic aberration) in electron (or ion) optical systems⁽⁶⁾, the only recourse is to image about the energy of greatest intensity.

Finally, intensity is a function of lens electrode aperture size and spacing. If for a particular positioning of object, image and lens the outer apertures of the lens are too large, then the electrostatic field bulging through them is distorted by object or image electrodes (or by interference from the magnetron field bulging through the K_2 aperture) with resulting aberration^(7,8) and hence, reduced image intensity. On the other hand, if the apertures are too small, only a small fraction of the source ions are intercepted by the lens, again resulting in image intensity reduction. Obviously a compromise must again be effected.

The above indicated lens limitations constitute problems reducible by optimum choice of lens design, positioning and operating parameters. However, it should be indicated that other limitations exist which are not so reducible. For example, a wide beam divergence results in spherical aberration for which there are no known solutions in electron optics⁽⁶⁾ and little recourse to minimizing

in the present situation. Finally, unless the lens is made to affect the field inside the magnetron, it can under the conditions assumed, supply no more than approximately 9 times the intensity available to the Q plate aperture by itself, with the latter placed adjacent to the source exit aperture. (This is the ratio of exit aperture area to Q plate aperture area.) The latter figure actually appears much too high. An intensity increase of 9 requires a magnification of $1/3$ and hence an image to object distance ratio of 3. This forces the lens back so that only a fraction of the beam solid angle emerging from the source can be intercepted by it; a maximum of unity magnification appears closer to the truth.

The above pessimistic conclusions are based on a necessarily pessimistic, general approach to the problem which must assume a broad, non-homocentric beam with a broad energy distribution (from an optical viewpoint). A beam more favorable to lens action may actually exist and the latter assumed problems may be minimal, hence the necessity for experimentation.

2. Design and operation:

Figures 1, 2 and 3 show the lens section, which consists of electrodes L_1 , L_2 , and L_3 . A design employing plane electrodes were chosen over cylindrical ones for compactness, versatility, and, for reduction of both spherical aberration and ionic space charge effects. The design chosen is that of an einzel lens which follows the proportions of the lens designed and studied by Zworykin⁽⁹⁾. As

previously discussed, the einzel lens has the advantage of focusing without increasing total ion energy, although the radial and axial components of this energy are changed. Selection of Zworykin's design has the advantage of making utilizable the focusing properties determined and plotted from his experimental data and giving assurance of an aberration-free design.

Lens focusing is accomplished by varying only the potential on L_2 . Electrodes K_2 , L_1 , L_3 and Q are kept at the same potential (ground) to provide a field-free region on each side of the lens⁽¹⁰⁾. This is essential to aberration-free performance since fields on either side of the lens would act to distort those of the lens itself. This arrangement also fulfills the zero potential requirements of the axis of the quadrupole analyzer.

Lens focal lengths can be determined from a graph published by Zworykin⁽¹¹⁾ and shown in Figure 4. As normally used for electrons, chart potentials V_C^* and V_0 correspond to the externally applied electrode potentials. This is because lens potentials (to a good approximation) are solely responsible for the electron's energy⁽¹²⁾, or potential per unit charge (V/e), within the lens. For the cold cathode ion source, however, ions have an initial spread of energies upon emerging from the source which are independent of lens electrode potentials. Ion energy within the lens is therefore the sum of the ions initial energy and that resulting from lens potentials.

Chart potentials were therefore determined by first assigning a negative electrode potential V_I to correspond to the ion's initial

* Not to be mistaken for the collector potential symbol V_C used elsewhere in the text.

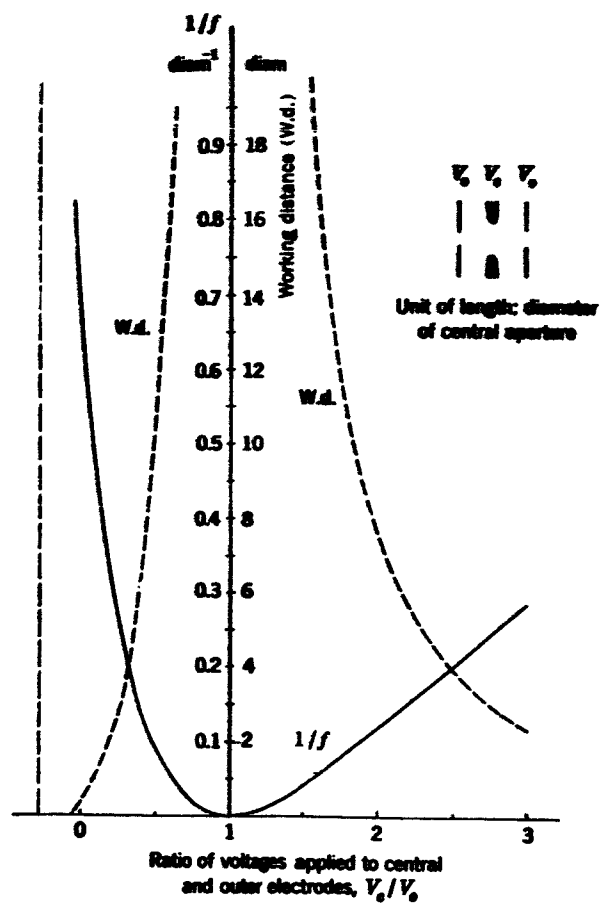


FIG. 4 GRAPH FOR DETERMINING FOCAL LENGTHS (FROM ZWORYKIN¹¹)

energy (e.g. $V_I = -30$ volts for a 30 ev ion). If V_{L1} and V_{L2} are the externally applied potentials to L_1 and L_2 , respectively, then, since V_{L1} is kept at zero volts,

$$\frac{V_C}{V_0} = \frac{V_I + V_{L2}}{V_I}$$

Figure 4 therefore indicates an infinite focal length for V_{L2} at zero volts and there is no lens action. The focal length decreases when V_{L2} is made either increasingly positive or negative. The focal length approaches zero for V_{L2} positive and approximately equal to V_I . However, for negative values of V_{L2} , $f \rightarrow 0$ only as $V_{L2} \rightarrow \infty$. Thus Figure 5 can be used to determine focal lengths for any combination of V_I and V_{L2} . When $V_C/V_0 > 3$, focal lengths can only be estimated.

II EXPERIMENTAL PROCEDURES AND AUXILIARY APPARATUS

Experimental source study was arranged into essentially three stages, subsequent to preliminary tests, as follows: (1) Measurement without a lens of ion current intensity vs energy as a function of (a) pusher cathode potential V_{K1} and (b) distance from the ion exit aperture K_2 . (2) Determination of lens effectiveness in improving sensitivity and (3) Measurement of ion current intensity vs energy as a function of gas composition and pressure.

The "Swagelok" fitting was used in stages (1) and (2). It allowed positioning of probe and lens via the positioning rod (Figure 2) without opening the flange and allowed each new distance between components to be measured externally. Completion of stages (1) and (2) allowed positioning to be fixed and allowed removal of the "Swagelok" teflon washers, to permit high temperature bake out of the source in preparation for stage (3).

Preliminary to experimental study, considerable care was exercised in aligning internal source components. This was critical for lens studies, since a narrowly focused beam might miss an off-centered probe aperture, for example. Critical elements of the magnetron and probe were assembled with the aid of alignment jigs. These centered and spaced the elements within their respective mounting cylinders. Lens elements were machine fitted. Subsequent to assembly, the entire source, including the lens, was centered in a lathe and alignment further checked with a cathetometer. Necessary adjustments were made by bending the kovar to glass supporting studs.

Prior to assembly, electronic components were polished to prevent high voltage breakdown, undesirable field emission and undesirable electrostatic field perturbations.

The vacuum system employed is shown schematically in Figure 5. A top view is shown photographically in Figure 6. The overall test set up is shown in Figure 7. The vacuum system was divided into upper and lower manifold units. This arrangement allowed the upper portion to be oven baked while being pumped from below. Subsequent to bake out, the upper manifold, thus cleaned, was valved off from the lower and pumped on itself.

The upper manifold consisted of the cold cathode ion source, a modulated Bayard-Alpert gauge, an 11 liter per second Ultek Model 10-252 ion pump, a Granville-Phillips Type L ultrahigh vacuum valve for valving off the upper manifold from the lower and a Varian valve for closing the ion pump. A Granville-Phillips thermostatically controlled oven was used for baking the upper manifold system.

The lower manifold consisted of a 20 l/sec Ultek model 10-354 ion pump, a 2400 l/sec mechanical pump, a port for feeding gas to the system and associated Granville-Phillips UHV valves for closing off the three outlets.

Energy spectra were obtained with the aid of a battery operated Keithley Model 600A electrometer. Measurements of collector current I_c vs collector potential V_c were made by insulating the electrometer from ground via a styrofoam block and reading currents with the case raised to the selected V_c values. Collector leakage currents,

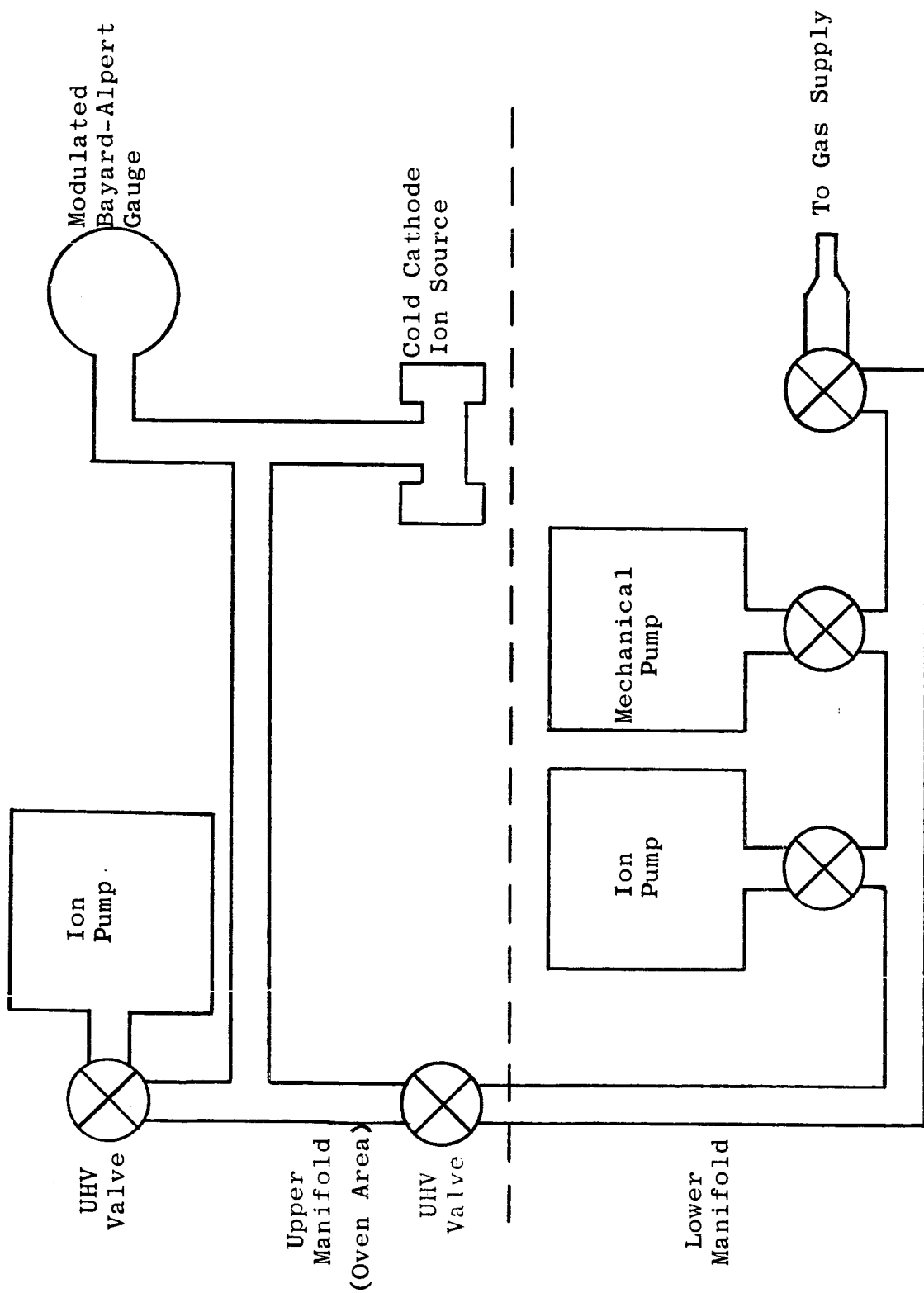


FIG. 5 VACUUM SYSTEM SCHEMATIC

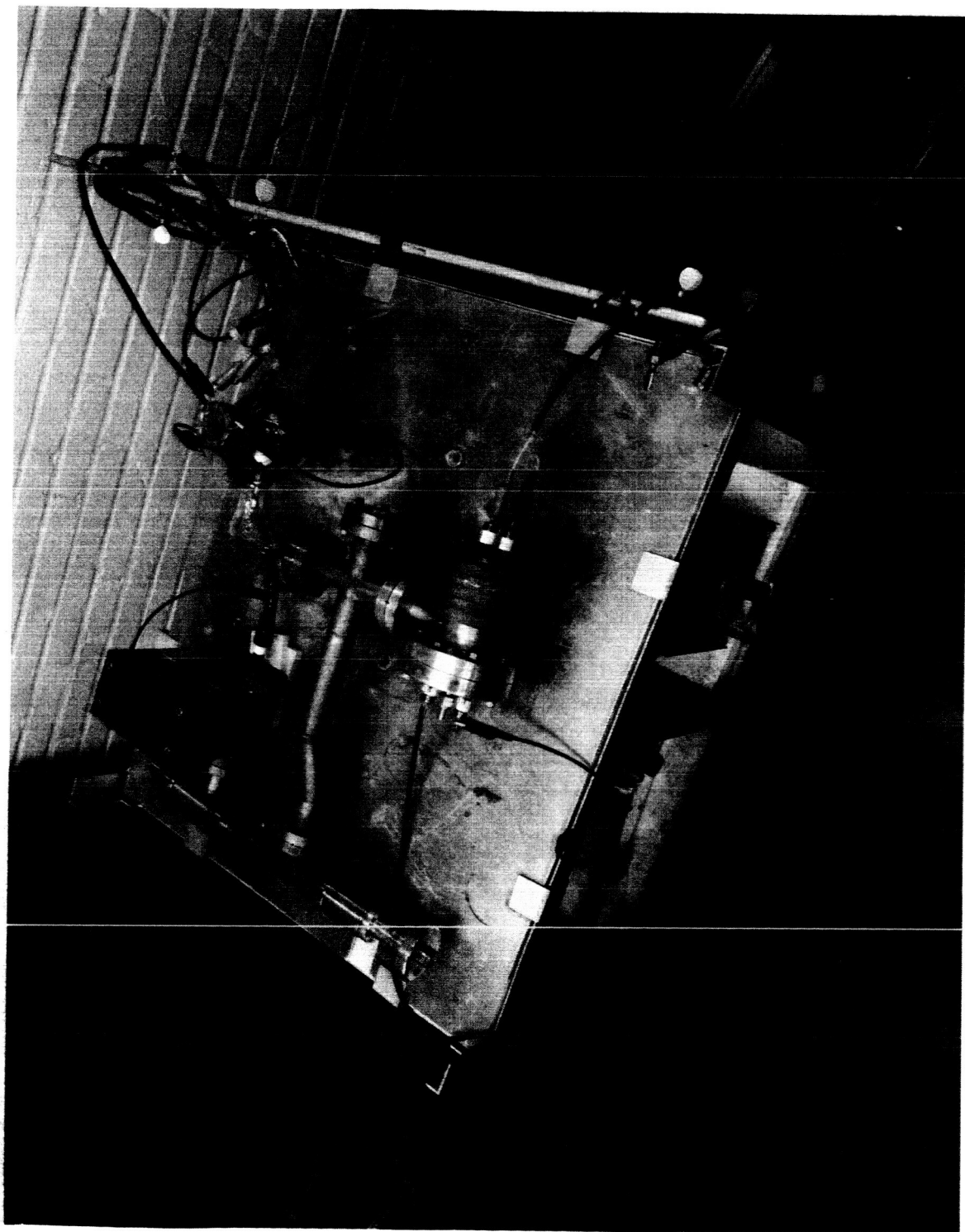


FIG. 6 VIEW OF THE UPPER MANIFOLD PORTION OF THE VACUUM SYSTEM

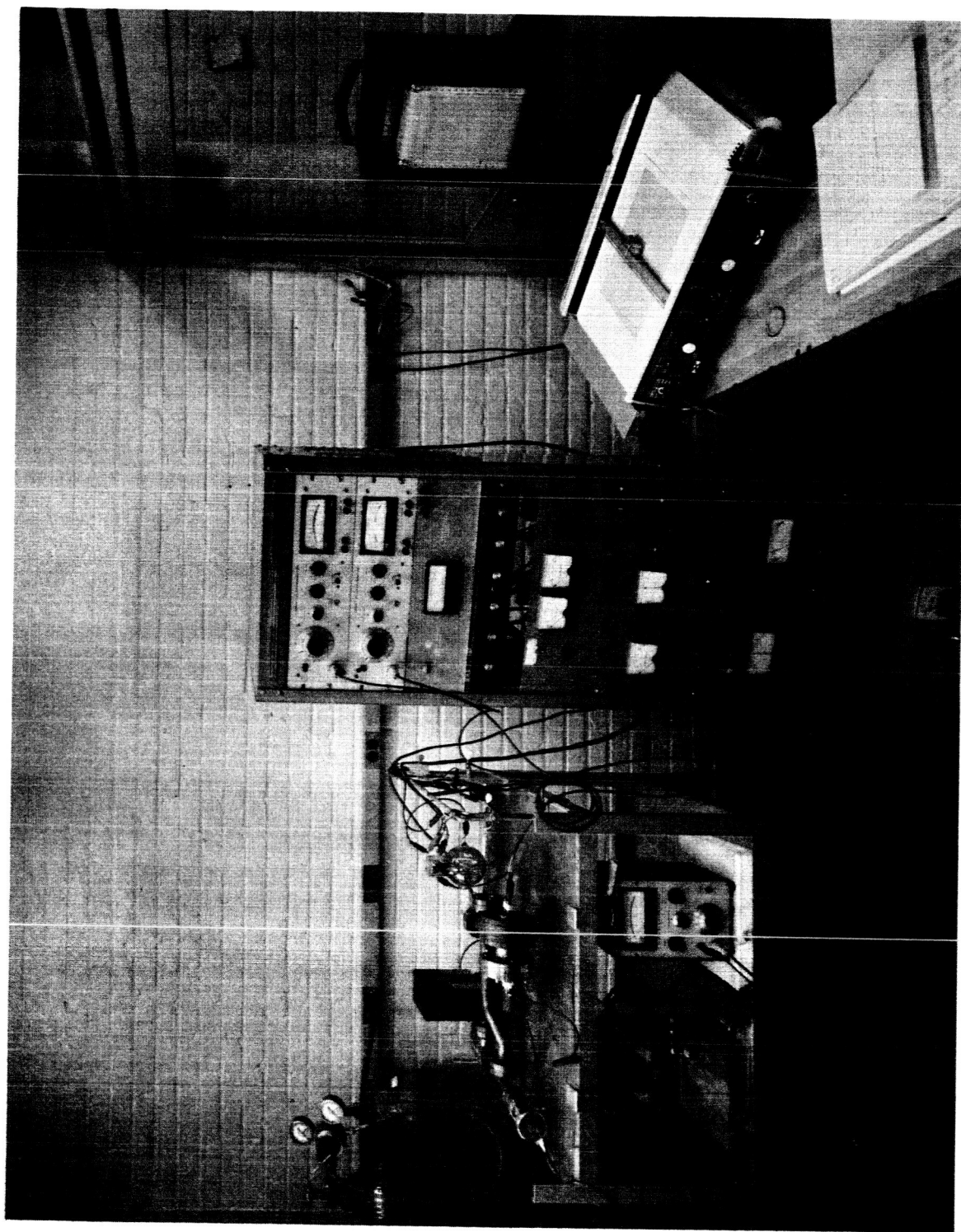


FIG. 7 VIEW OF VACUUM SYSTEM AND ASSOCIATED ELECTRONICS

obtained with the anode potential off, were subtracted from collector current readings after each set of readings were obtained.

Keithley Model 610 electrometers monitored the remaining electrode currents I_Q and I_{K1} . A Moseley (Model 2D-2A) X-Y recorder proved expeditious for recording source characteristics during the lens experiments.

Magnetic field measurements were made prior to source studies and again during lens experiments.

III EXPERIMENTAL RESULTS AND CONCLUSIONS

A. Ion Beam Studies Without the Lens

1. Ion energy distribution vs V_{K1} :

Initial experiments were concerned primarily with determining which value of pusher cathode potential V_{K1} would provide the highest ion beam intensity through the Q aperture and with determining the resulting ion (and electron) energy distribution. The results of these experiments are shown in Figure 8. Collector current I_c is plotted vs collector potential V_c for $-110 < V_c < +110$ volts and for $-40 < V_{K1} < +40$ volts.

The K_2 to Q distance chosen was 0.61 inches, approximately the same as used in the feasibility study. Anode potential was 5.6 KV and the mean pressure was 5.5×10^{-8} torr (Nitrogen). The axial magnetic field at the center of the magnetron was 1225 gauss (magnetic field values given in the October report were in error).

The curves for positive V_c display steep slopes initially, gradually leveling off as V_c increases. This indicates a predominance of low energy ions for all values of V_{K1} , enabling high quadrupole analyzer sensitivity. Highest sensitivities are indicated for $V_{K1} \leq 0$, since the ratio of differential collector current to differential retarding potential ($\Delta I_c / \Delta V_c$) is then greatest. However, a predominant electron component is also indicated for $V_{K1} \leq 0$. This is evidenced by the negative I_c values at zero V_c . For negative values of V_{K1} reliably to represent a quantitative ion energy distribution, it is therefore essential that the electron current passing

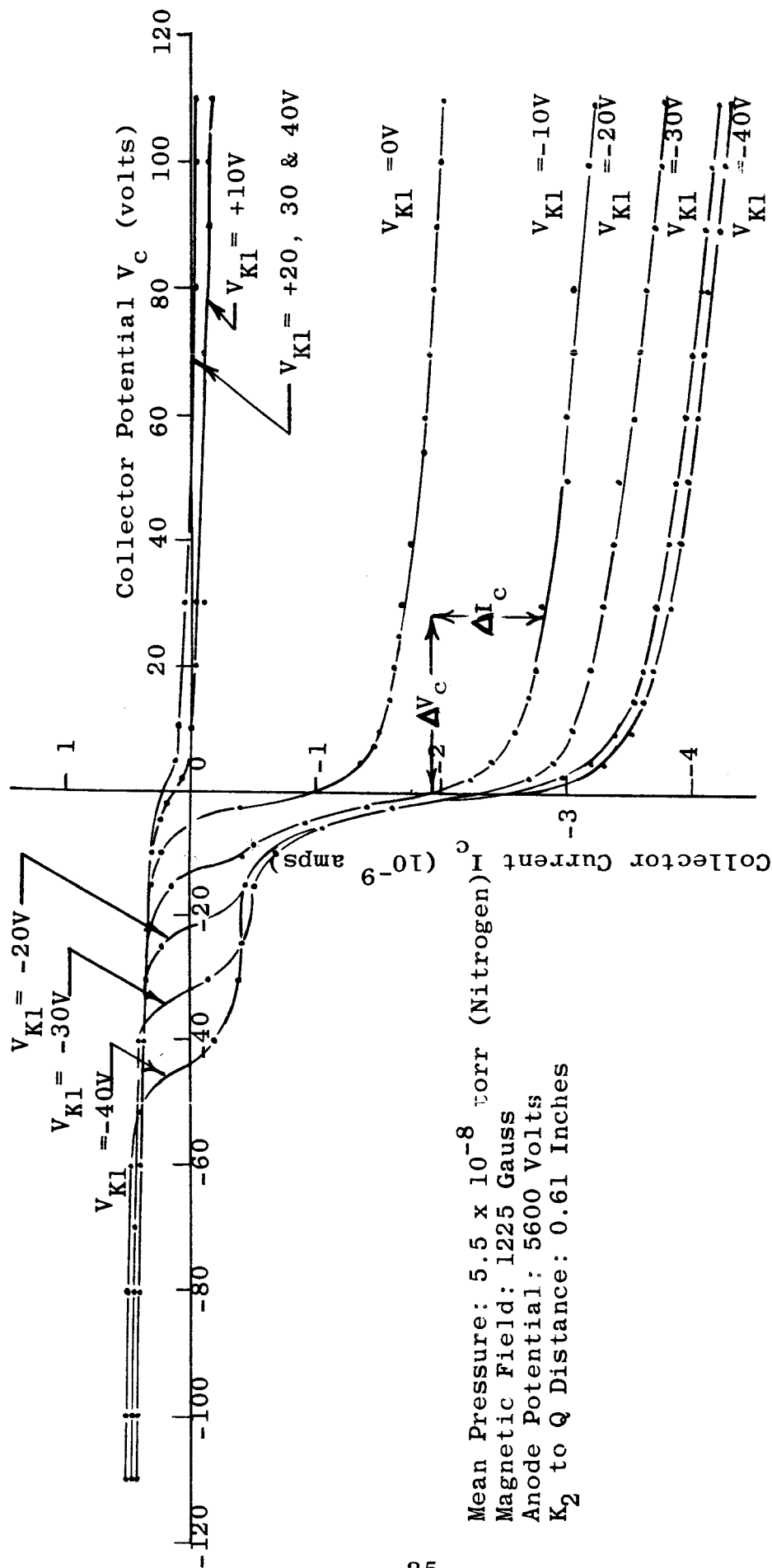


FIG. 8 COLLECTOR CURRENT VS COLLECTOR POTENTIAL FOR SELECTED PUSHER CATHODE POTENTIALS (V_{K1})

through Q remain constant for all positive values of V_c .

Although Helmer and Jepson⁽¹³⁾ apparently assumed a constant electron current when probing the ion energy distribution of a Penning source having a large electron component, it was considered essential to investigate this situation experimentally. For this purpose, data on I_c vs negative V_c , shown in Figure 8 was taken. The verification sought was based in the following reasoning:

If the electron component remains constant for positive V_c , then the ion component must remain constant for negative V_c . At some negative value of V_c , when all electrons are retarded, the total ion current will be indicated as the absolute value of I_c . This value must therefore equal or exceed the ion current, ΔI_c , indicated for positive values of V_c , over some range ΔV_c .

Over the negative V_c range investigated, the data of Figure 8 fails to give the sought after verification.. For $V_c < -50$ volts, collector current is essentially constant and independent of V_{K1} . The data therefore indicates that essentially all electrons have been retarded. Hence a total ion current of approximately 0.5×10^{-9} amperes is indicated. This fails to equal or exceed ion currents indicated for positive V_c , when $V_{K1} \leq 0$. For example, for $V_{K1} = -40$ volts and $\Delta V_c = 100$ volts ($0 < V_c < +100$ volts), $\Delta I_c = 1.8 \times 10^{-9}$ amperes.

Two explanations are possible. One is that some electrons have not been retarded due to the presence of a higher energy component, this would mean that the plateau value of I_c does not represent total ion current. The other explanation (possibly in combination with the first) is that the change in I_c with positive V_c is caused by drawing in increasing numbers of electrons through Q as V_c is made increasingly positive. Lens study data, discussed in IIIB, supports the latter explanation. However, a careful extension of the data to values of $\pm V_c$ in the vicinity of anode potential might be required to answer these questions more completely.

In Figure 9, differential collector currents, obtained from the data of Figure 8, have been plotted against V_{K1} for selected intervals of retarding field potentials. In view of the above discussion, only those currents plotted for positive values of V_{K1} can be considered a valid quantitative representation of ion beam current as a function of energy (only small electron components are indicated for these values in Figure 8). The values shown for negative V_{K1} are probably too high, although possible. Very likely, they are of the same order of magnitude as those of positive V_{K1} . Values of I_c are shown to be essentially independent of positive values of V_{K1} . The percentage of the beam made up of particular energy ions is shown to be essentially invariant with V_{K1} , with low energy ions predominating.

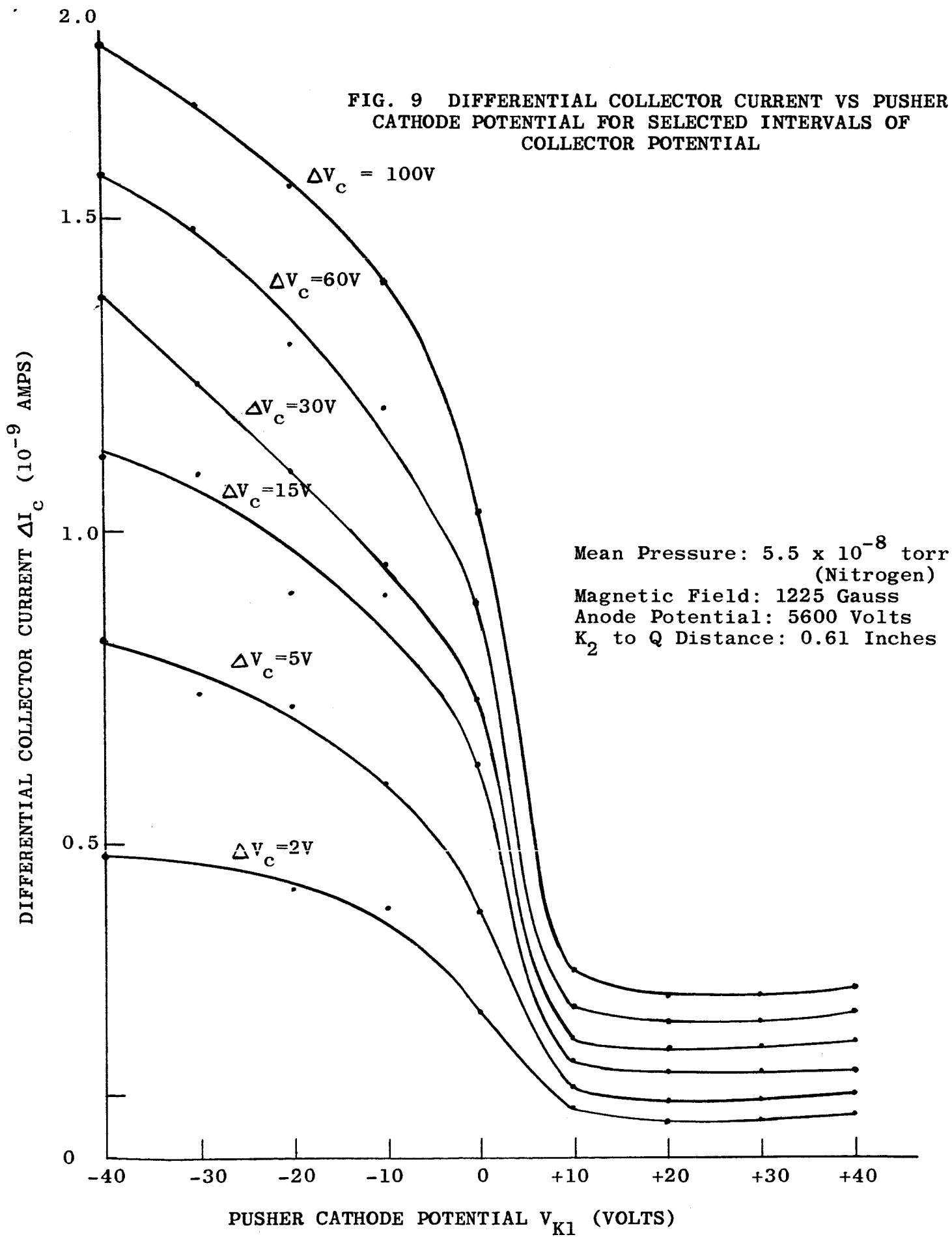
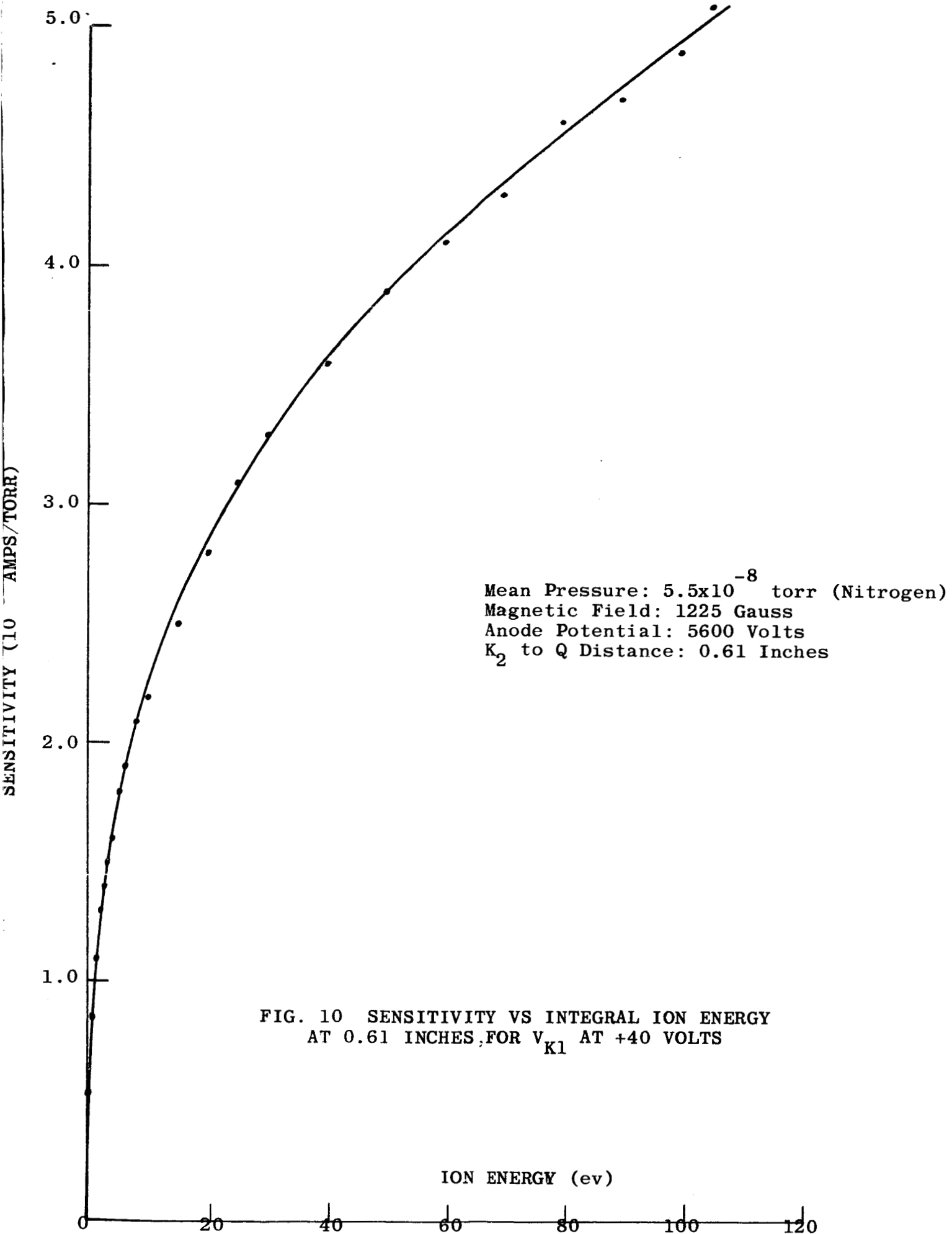


Figure 10 shows a typical integral ion energy spectrum indicated by the data of Figure 8. Ion beam sensitivity in amps/torr is plotted against ion energy for $V_{K1}=+40$ volts. It is seen for example that ions between zero and 30 ev constitute about 2/3 of the ions under 100 ev while ions between zero and 10 ev constitute about half.

2. Ion energy distribution vs distance:

In view of the above discussed lack of evidence of a convincing sensitivity advantage of one value of V_{K1} over others, studies of ion energy spectra vs distance were conducted with $V_{K1}=+40$, zero and -40 volts. The results of these studies are shown in Figures 11, 12 and 13 respectively. Differential collector current between zero V_c and selected positive values is shown over a K_2 to Q distance range of 0.14 inches to 1.83 inches.

Conditions are essentially the same as in previously discussed data including a mean pressure of 5.5×10^{-8} torr. However, there is a pressure variation of $\pm 0.3 \times 10^{-8}$ torr. (The data shown at 0.61 inches is taken from the data of Figure 8, already discussed). Difficulties were encountered with what appeared to be changes in operational mode. As a result, cathode current I_{K1} was observed to change by as much as 35%. While care was taken to preserve the same mode for all data taken, there is doubt about the mode for $V_{K1}=+40$ volts at 0.88 inches (Figure 11). The indicated current therefore may be in error by as much as $\pm 35\%$.



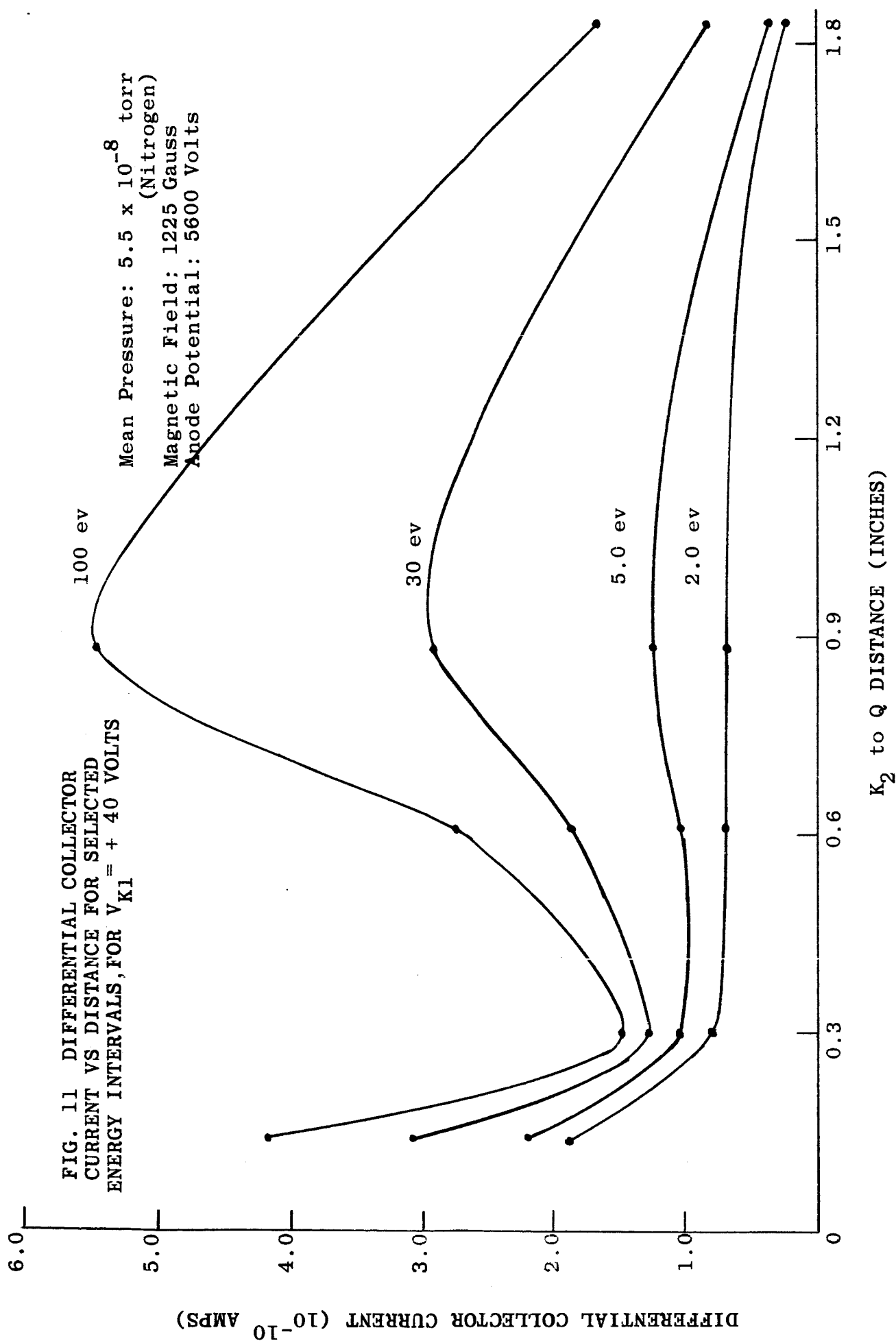


FIG. 12 DIFFERENTIAL COLLECTOR CURRENT
VS DISTANCE FOR SELECTED ENERGY INTERVALS,
FOR $V_{K1} = \text{ZERO VOLTS}$

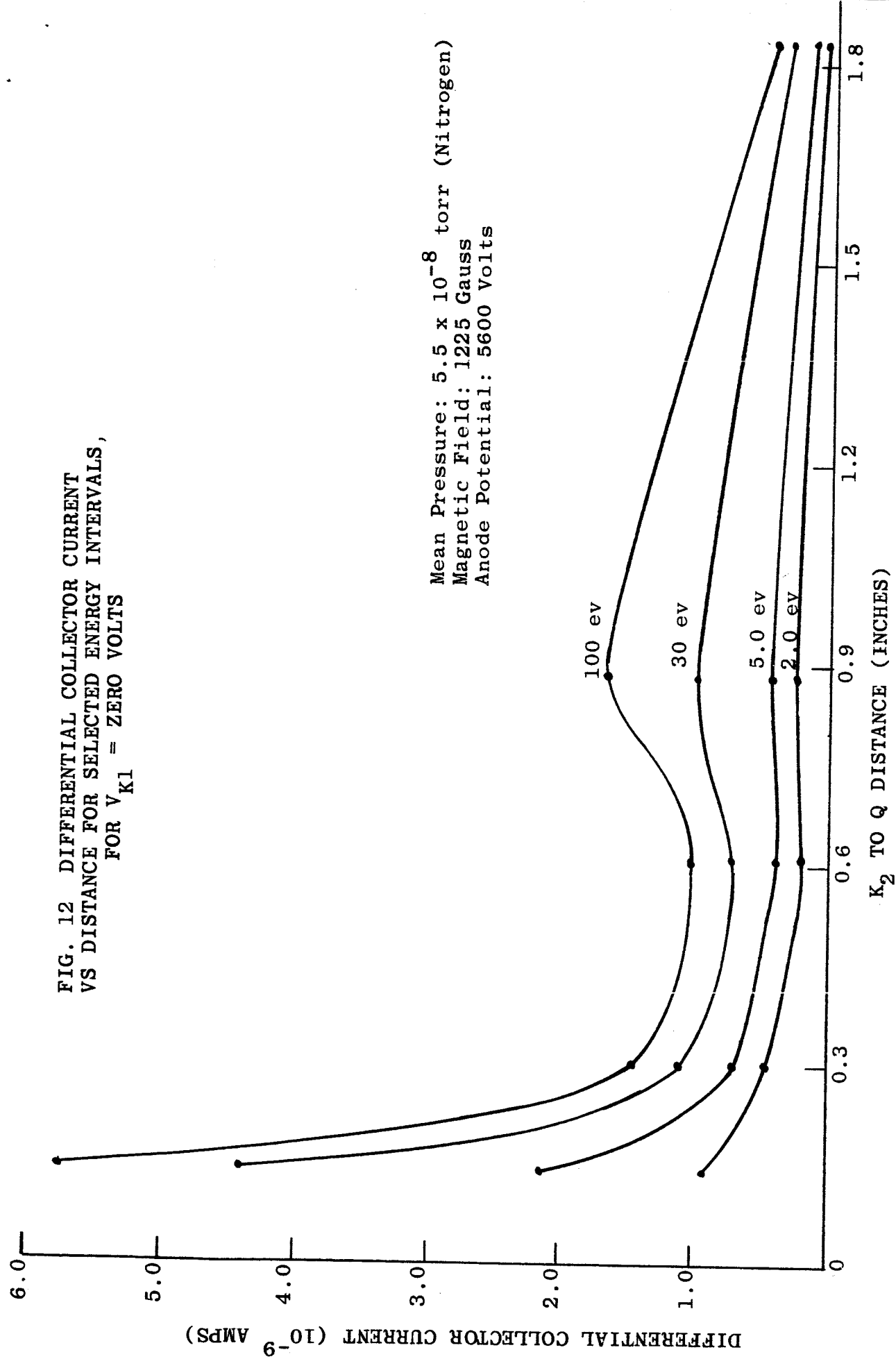
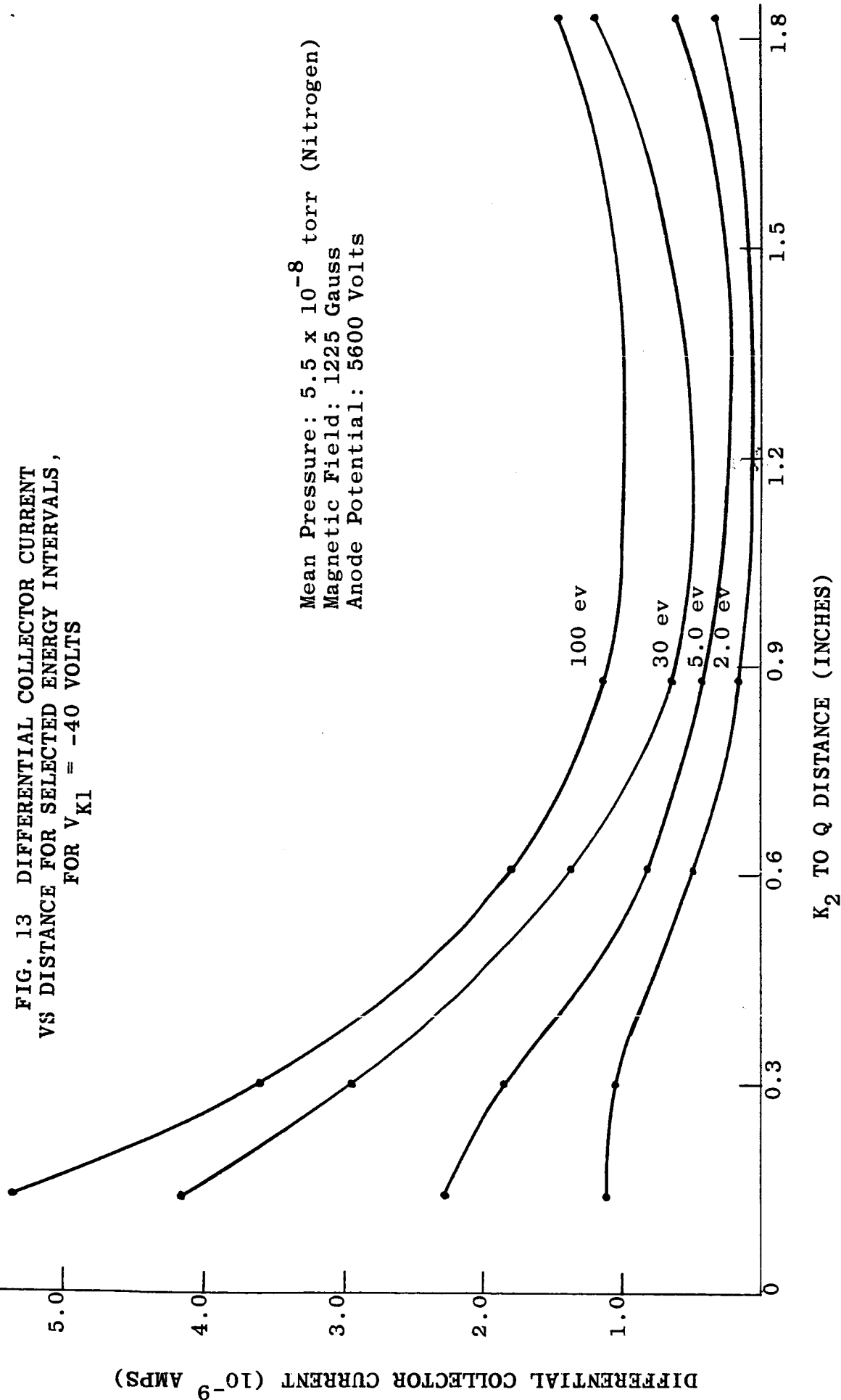


FIG. 13 DIFFERENTIAL COLLECTOR CURRENT
VS DISTANCE FOR SELECTED ENERGY INTERVALS,
FOR $V_{K1} = -40$ VOLTS

Mean Pressure: 5.5×10^{-8} torr (Nitrogen)
Magnetic Field: 1225 Gauss
Anode Potential: 5600 Volts



For all three values of V_{K1} , the highest differential collector current is seen to be obtained nearest the beam exit aperture, (with the exception of values for $V_{K1}=+40$ at a distance of 0.88 inches for $V_c > 30$ volts). A current peak also occurs at a point more distant. For $V_{K1} =$ zero volts and +40 volts the second peak is approximately at 0.88 inches, while for $V_{K1}=-40$ volts it is further but less precisely indicated (due to the limited data obtained). The precise energy distribution is seen to vary with both distance and V_{K1} . However, low energy ions are indicated to predominate over all values of V_{K1} and distance in a manner approximating that shown in Figure 10.

Considering ions with energy < 30 ev as an example, the highest indicated sensitivities are 5.5 ma/torr for $V_{K1}=+40$ volts, at distances of both 0.14 inches and 0.88 inches. For $V_{K1}=0$ volts and -40 volts the indicated sensitivities are 80 ma/torr and 76 ma/torr respectively, both at 0.14 inches. However, in view of the large electron component present for the latter two V_{K1} values, their sensitivity figures are probably too high, as discussed earlier.

The more conservative figure of 5.5 ma/torr obtained for $V_{K1}=+40$ volts at a distance of either 0.14 inches or 0.88 inches compares with 5.1 ma/torr obtained with the source used in the feasibility study. Since the latter used a Q aperture (then called A-2) nine times the area of the present one, a minimum sensitivity improvement of a factor of 10 is indicated without the use of a lens.

B. Lens Effectiveness

Three positions of lens and probe were selected for experimentation, as follows:

1. K_2 to $L_2 = 1.38''$ and K_2 to $Q = 1.83''$. This constitutes an object distance (K_2 to L_2) approximately three times the image distance (L_2 to Q) to provide a $1/3$ magnification of the K_2 exit aperture at Q . A minimum of one L_3 aperture diameter was left between L_3 and Q to prevent distortion of the lens field and consequent aberration.

2. K_2 to $L_2 = 0.82''$ and K_2 to $Q = 1.63''$. This constitutes the closest proximity between K_2 , lens and Q for largest beam fraction interception without lens field perturbation, either by the magnetron field or adjacent electrodes. In the event of a nearly parallel beam, nearly all ions would be focused into Q (discounting aberrations) by making Q the focal point.

3. K_2 to $L_2 = 0.46''$ and K_2 to $Q = 0.90''$. This constitutes approximately the closest distance between K_2 , the lens and Q possible without the three physically touching each other. The largest beam fraction is thereby intercepted by the lens while Q is also closest for maximum demagnification, which in this case is unity. There is no regard for field perturbations by electrode or magnetron field proximity and the importance of such aberrations vs the importance of intercepting a larger fraction of ion beam is thereby tested. The possibility exists of lens interaction with the field of the magnetron for extraction of a larger number of ions

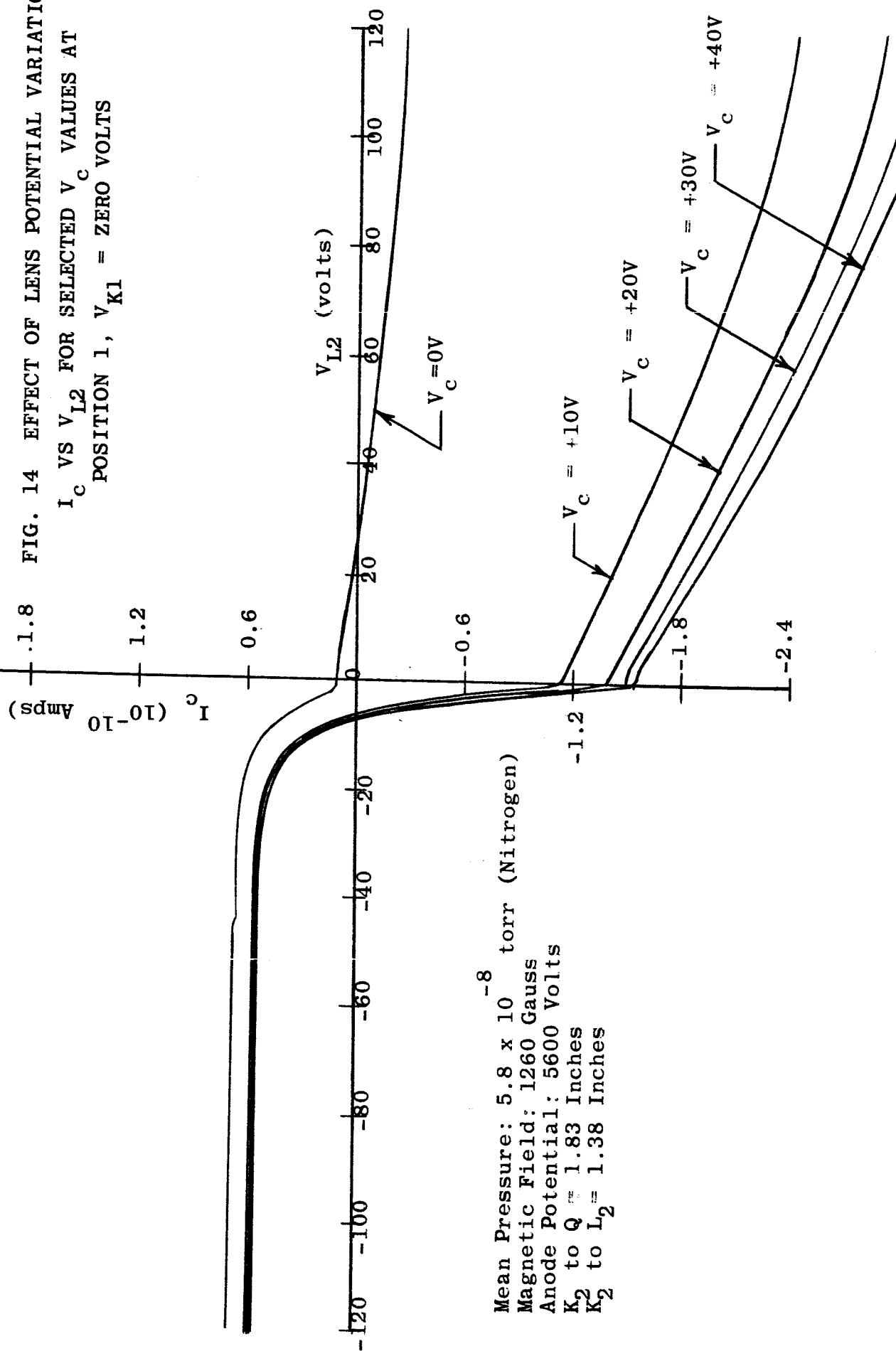
and of focusing a near parallel beam into Q (Magnification is then unimportant).

By varying lens potentials over several hundred volts, the requisite focal distances for the indicated positions should be attainable. This is discussed in Section ID together with a fuller discussion of the reasons underlying the choice of the experimental conditions selected and of expected lens performance limitations.

Examples of data obtained at position I is shown in Figures 14 and 15 for V_{K1} = zero and +40 volts, respectively. Collector current I_c is shown plotted against lens potential V_{L2} for $-120 < V_{L2} < +120$ volts. This was done for several values of retarding potential V_c , as shown, to note the effect on ions of different energies, since focusing will be energy dependent. Other conditions are essentially the same as for previously discussed experiments without the lens.

It is seen in Figure 14 and to a lesser extent in Figure 15 that the ratio of differential collector current to differential retarding potential, $\Delta I_c / \Delta V_c$, increases as V_{L2} becomes more positive and decreases as it becomes more negative. Superficially, this appears to indicate ion focusing and ion defocusing, respectively. However, such behavior seems highly unlikely. An important reason is that low energy ions are indicated to be convergent long after V_{L2} is sufficiently positive to retard them; e.g., 10 ev ions (indicated by I_c for $0 < V_c < 10$ volts) are still shown increasing when

FIG. 14 EFFECT OF LENS POTENTIAL VARIATIONS:
 I_c VS V_{L2} FOR SELECTED V_c VALUES AT
 POSITION 1, V_{K1} = ZERO VOLTS



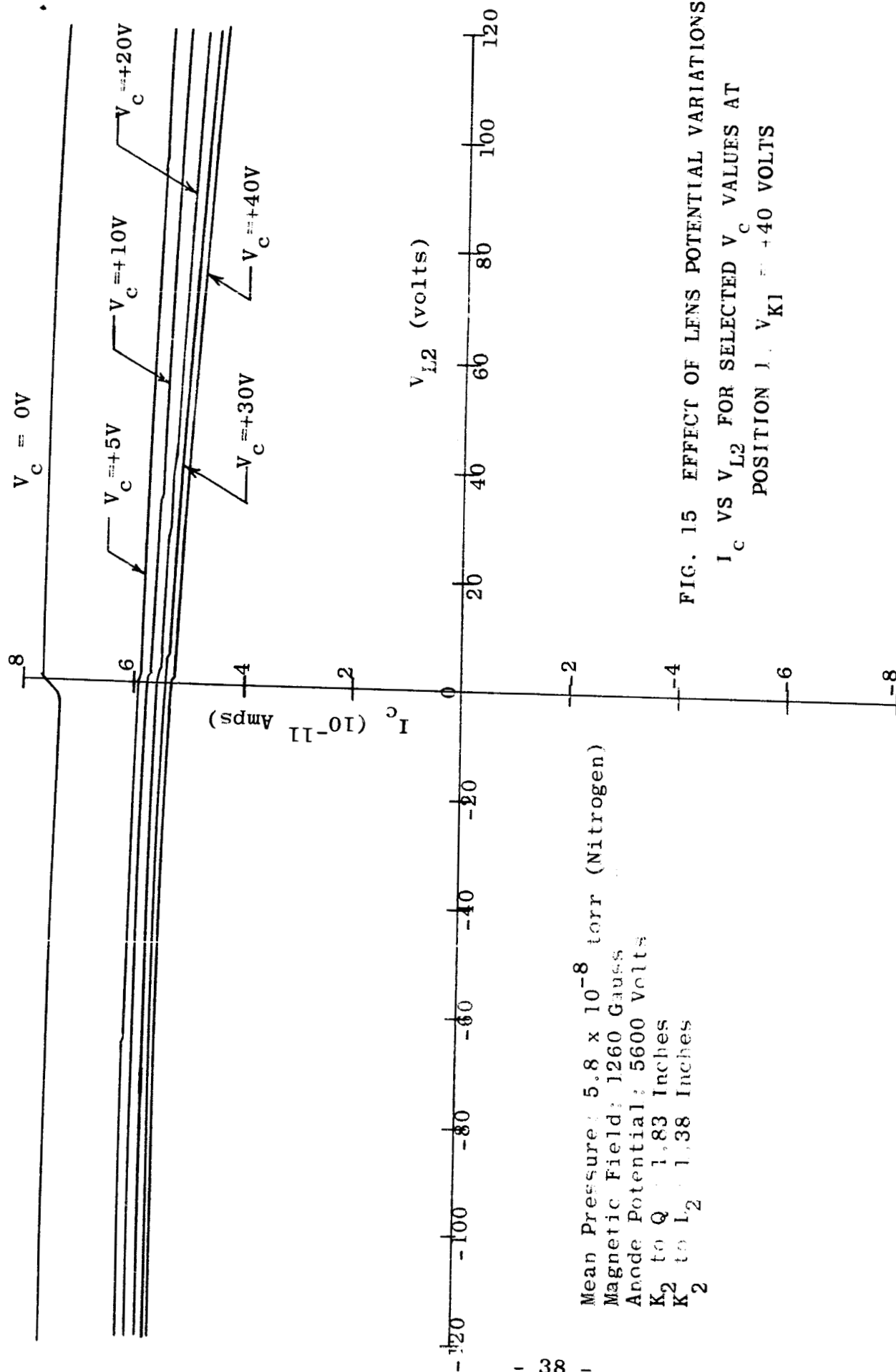


FIG. 15 EFFECT OF LENS POTENTIAL VARIATIONS:
 I_c VS V_{L2} FOR SELECTED V_c VALUES AT
 POSITION 1, $V_{K1} = +40$ VOLTS

Mean Pressure: 5.8×10^{-8} torr (Nitrogen)
 Magnetic Field: 1260 Gauss
 Anode Potential: 5600 Volts
 K_2 to Q : 1.83 Inches
 K_2 to L_2 : 1.38 Inches

V_{L2} is +120 volts.

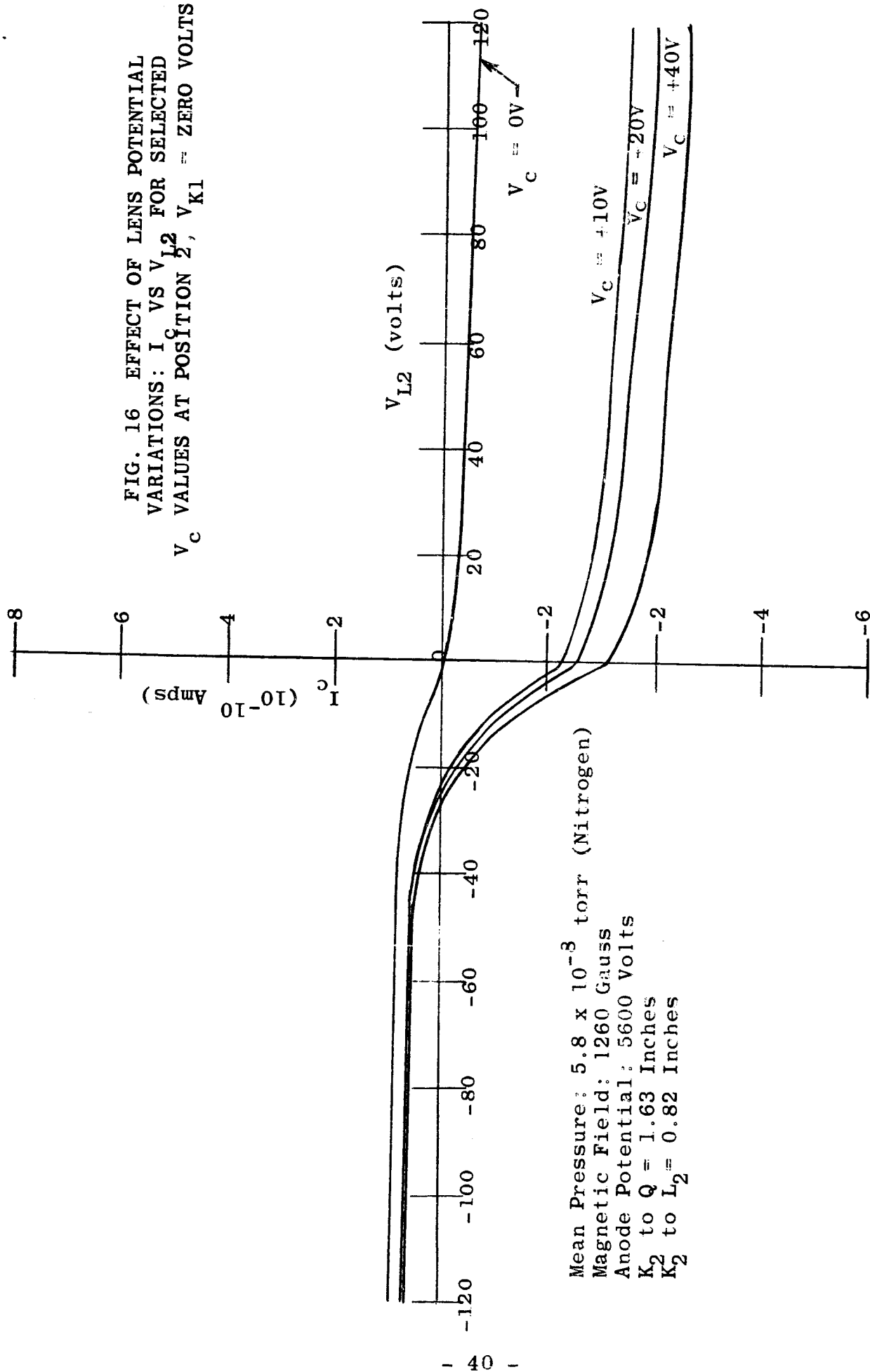
This anomalous behavior can be accounted for by the focusing of electrons in the beam. For $V_{K1}=0$ (Figure 14), this effect predominates over ion focusing, over the V_{L2} range shown. Electron focusing is evident because I_c goes negative as V_{L2} goes positive even when $V_c=0$. However, as indicated by previous data obtained without the lens, electrons also appear to be drawn through Q when V_c is made positive. Therefore, when V_{L2} is made increasingly positive this effect would be enhanced and thus account for the apparent increase in ion current. For $V_{K1}=+40$ (Figure 15) this effect is smaller since there are fewer electrons in the beam.

When V_{L2} is made negative, low energy electrons are eventually repelled. Figure 8 shows that at $V_{K1}=0$ the electrons (or their low energy component) have a maximum energy of about 20 ev. In Figure 14 ΔI_c decreases until V_c is approximately -20 volts. This indicates that only at that point is ΔI_c purely ionic. The latter effect is pronounced for $V_{K1}=0$ volts because of the predominant electron beam component. This effect also accounts for the increase in I_c at $V_c=0$, where V_{L2} goes negative. For $V_{K1}=+40$ volts, the effect is negligible due to the very small electron component. Thus, much of the anomalous ion defocusing, shown for negative V_{L2} , appears accounted for.

The focusing pattern of position 1 was repeated for position 2, as indicated in Figure 16.

While a complete understanding of this complicated situation

FIG. 16 EFFECT OF LENS POTENTIAL
VARIATIONS: I_c VS V_{L2} FOR SELECTED
 V_c VALUES AT POSITION 2, $V_{K1} = \text{ZERO VOLTS}$



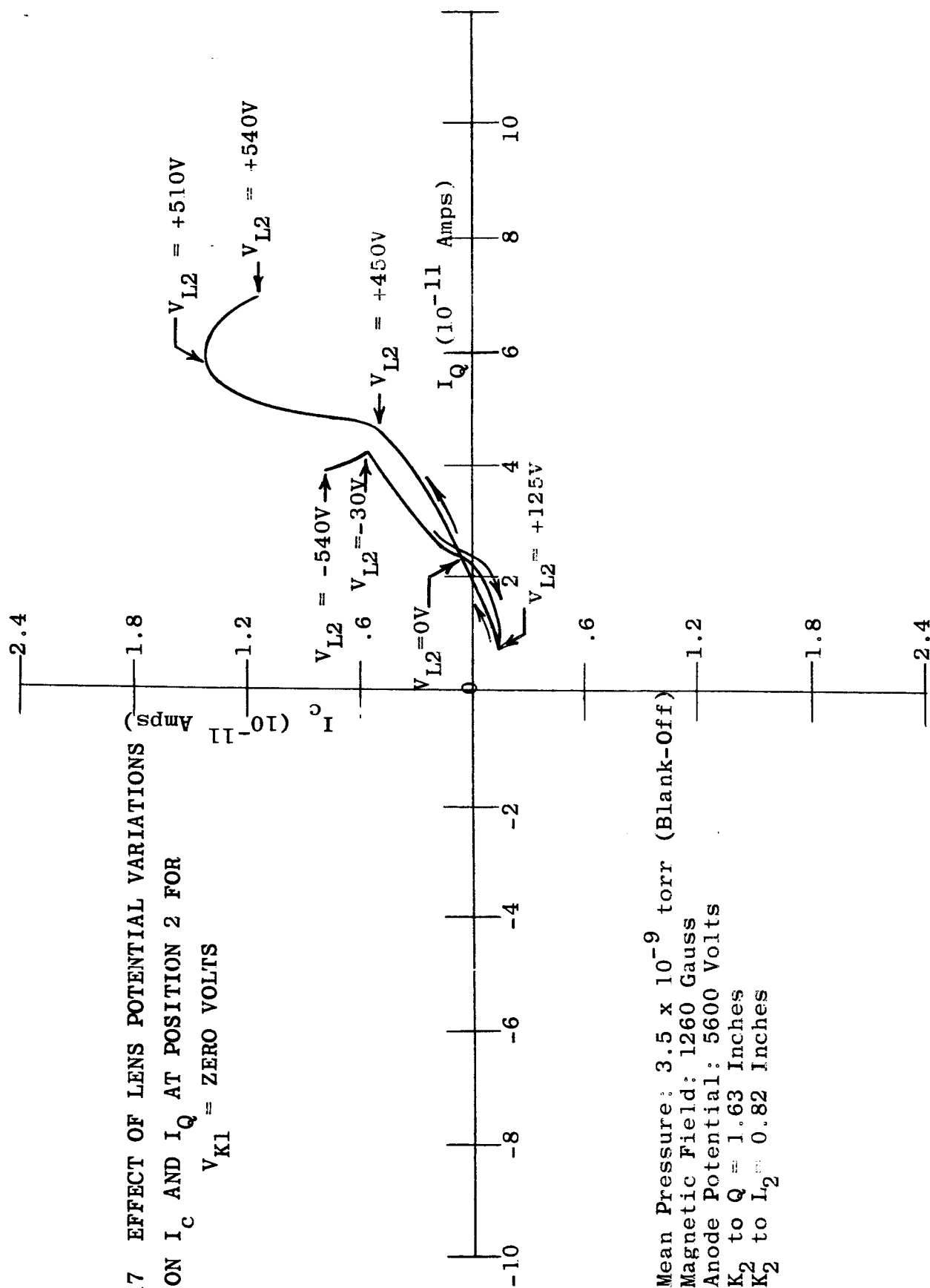
would require perhaps considerably more study, it must be concluded that the lens provides no reliable improvement in ion sensitivity. This possibility was anticipated and a number of reasons for it discussed in Section ID.

Focusing was also investigated by plotting collector current I_c against Q aperture current I_Q as a function of V_{L2} .

This was based on the reasoning that when focusing occurs, it must be indicated by both a maximum positive I_c and by a maximum I_c/I_Q ratio. A wider range of lens potentials were used here, in consideration of the possibility that a space charge effect in the lens might be altering its equipotential distributions.

A representative curve obtained for position 2 is shown in Figure 17, for $V_{K1}=0$ volts. Arrows along the curve indicate the direction taken by the data as V_{L2} was varied from 0 to +540 volts and from 0 to -540 volts. Ion focusing is indicated for both positive and negative values of V_{L2} . The most intense focusing is indicated for positive V_{L2} with a peak occurring at $V_{L2}=+510$ volts. However, I_c vs V_c curves obtained for $V_{L2}=+510$ volts showed no improved ion current sensitivity in the energy range of interest. The same results were obtained for $V_{K1}=+40$ volts and -40 volts.

The focusing curve obtained at position 3 is shown in Figure 18; it includes data for $V_{K1}=0, -40$ and $+40$ volts. Figure 19 shows the associated I_c vs V_c curves obtained at these focusing potentials, for $-40 < V_c < +40$ volts. As before, no improvement in ion current



Mean Pressure: 3.5×10^{-9} torr (Blank-Off)
Magnetic Field: 1260 Gauss
Anode Potential: 5600 Volts
 K_2 to $Q = 1.63$ Inches
 K_2 to $L_2 = 0.82$ Inches

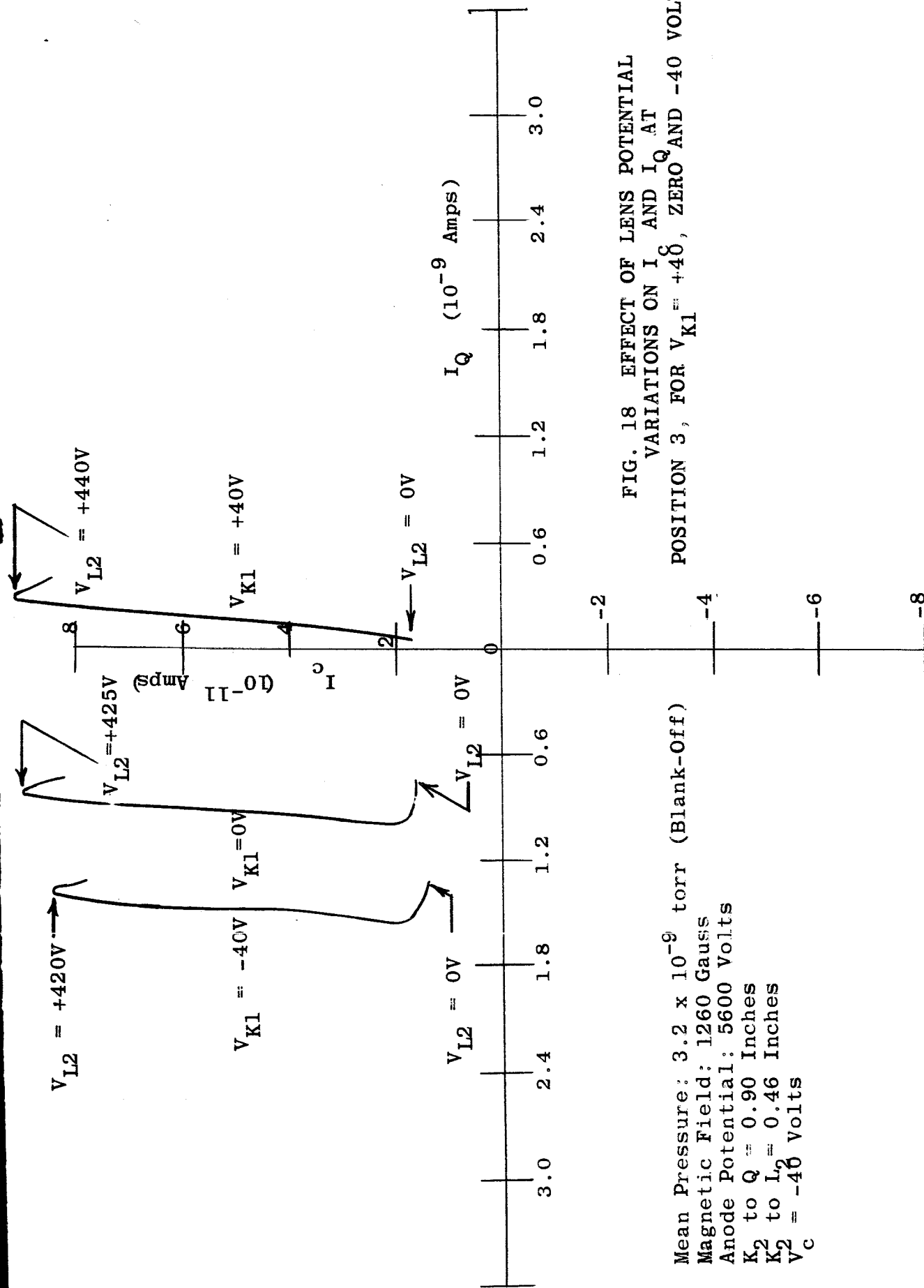


FIG. 18 EFFECT OF LENS POTENTIAL VARIATIONS ON I_c AND I_Q AT POSITION 3, FOR $V_{K1} = +40$, ZERO AND -40 VOLTS

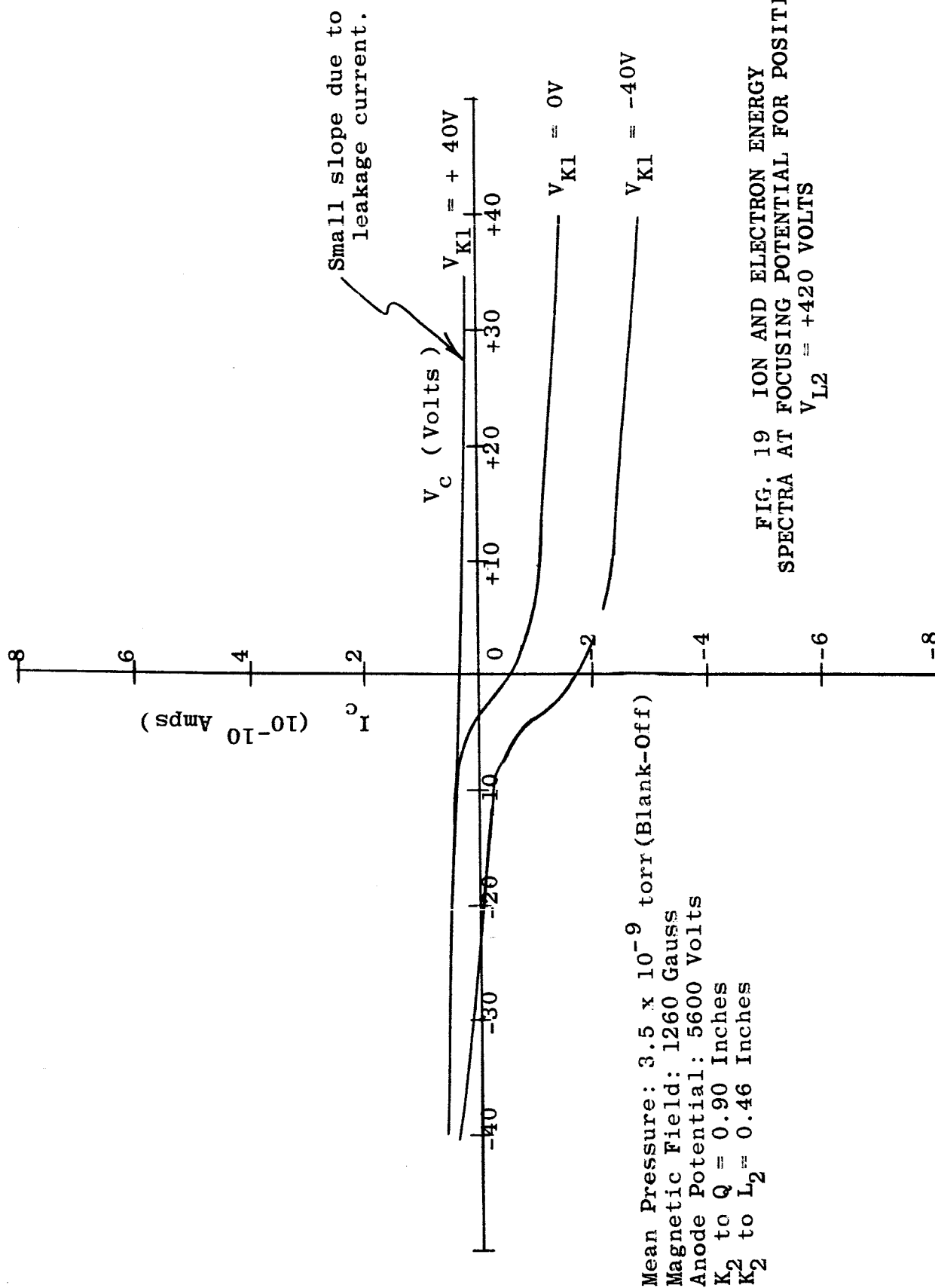


FIG. 19 ION AND ELECTRON ENERGY
 SPECTRA AT FOCUSING POTENTIAL FOR POSITION 3:
 $V_{L2} = +420$ VOLTS

sensitivity is evident at these low energies. (On the contrary, this approach has led to a decided ion current decrease.)

C. Vacuum Performance Characteristics

Subsequent to the above studies, the instrument was prepared for the final stage of experimentation, requiring clean up of the source and system for operation well below 10^{-9} torr. This phase is primarily concerned with determination of the behavior of ion collector current as a function of pressure and determination of the effects on the ion energy distribution of gas composition.

The design originally called for replacement of the "Swagelok" connector with a ceramic feedthrough after sensitivity studies were performed. However, it was decided that dummy "Swagelok" fittings, substituting steel washers for teflon, would enable high temperature bake out, while lens or Q plate feedthroughs could be used for the collector.

Unfortunately, subsequent to high temperature bake out of the source with the latter arrangement, leaks developed in three of the feedthroughs. Repeated attempts at repairing them without hazarding new feedthrough welding operations proved unsuccessful. It was therefore impossible to conduct the gas composition and linearity studies under this contract. (Sensitivity of I_c and I_{K1} vs pressure was checked and found to be linear between 1×10^{-8} and 5×10^{-8} torr.)

IV QUADRUPOLE MASS SPECTROMETER DESIGN

A. Summary of Design Criteria

Reasons for selection of the quadrupole analyzer, discussion of its general design criteria and mass scanning modes, as well as associated references are contained in the final report for Contract NAS1-2691, Task 2⁽³⁾. The following design equations and mode selection are taken from that report.

The quadrupole mass analyzer is illustrated in Figure 20 together with ion source and ion detector; symbols used in the following discussion are also indicated. The analyzer consists of four rods with superimposed steady state and r.f. potentials on each. The r.f. potential on one pair of rods is 90° out of phase with the other pair. Operation derives from the motion of ions in the field of these rods. The descriptive equations of their motion, using cartesian coordinate axes x, y and z, are

$$(1) \quad M\ddot{x} + e(U+V \cos 2\pi\nu t) x/r_o^2 = 0$$

$$(2) \quad M\ddot{y} - e(U+V \cos 2\pi\nu t) y/r_o^2 = 0$$

where M = mass of the ion

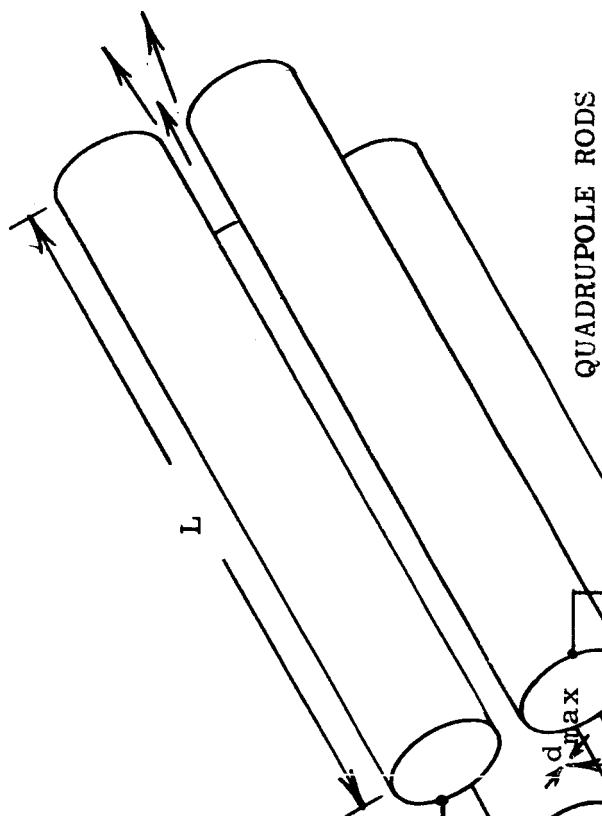
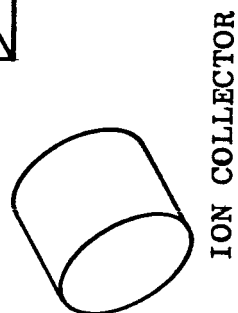
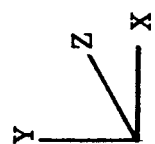
U = steady state rod potential

V = r.f. rod potential

ν = frequency of the V potential

e = electronic charge on the ion

r_o = radius of circle inscribed by the four rods



ION
SOURCE

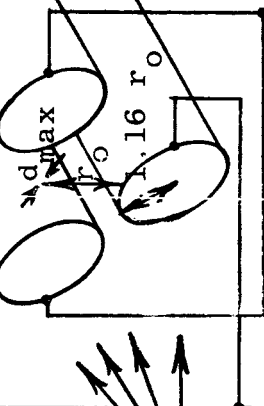
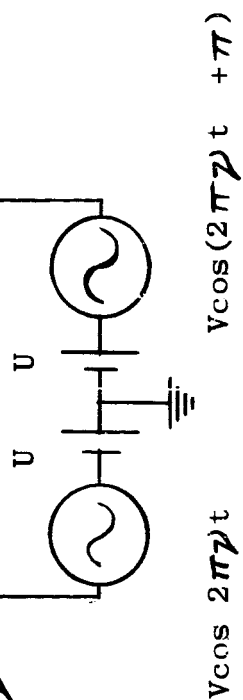


FIG. 20 SCHEMATIC OF QUADRUPOLE
MASS ANALYZER



Ion trajectories, determined from the solution of these equations may be either stable or unstable. If unstable, or if stable with amplitude $\geq r_0$, the ions will be captured by the rods after a sufficient number of cycles or the r.f. field. The filtering process operates by providing stable, bounded paths only for the mass selected. A stable trajectory exists if

$$(3) \quad M = 2.30 \times 10^{-20} V/\nu^2 r_0^2$$

A mass spectrum is thus scanned by varying V and/or ν . (MKS units are used unless otherwise stated).

Three scanning modes have been described in the literature. The mode selected requires the mass peak width, ΔM , to remain constant. Since the resolution is determined from

$$(4) \quad \frac{M}{\Delta M} = \frac{0.126}{0.16784 - U/V}$$

the selected scanning mode and a choice of 1 amu for ΔM requires that

$$(5) \quad U = 0.1678 V - 9.10 \times 10^{-9} \nu^2 r_0^2$$

For a fixed peak width, 100% transmission of stable ions can be obtained by satisfying the following conditions:

$$(6) \quad \text{Potential stability} = \frac{1}{2} \left(\frac{\Delta M}{M} \right)$$

$$(7) \quad \text{Frequency stability and dimensional accuracy} = \frac{1}{4} \left(\frac{\Delta M}{M} \right)$$

$$(8) \quad U_{Tmax} = \frac{V}{15} \left(\frac{\Delta M}{M} \right)$$

where U_{Tmax} = maximum transverse energy of ions injected on axis (in electron volts).

$$(9) \quad U_{Amax} = 5.82 \times 10^{-3} \frac{L^2 V}{r_o^2} \left(\frac{\Delta M}{M}\right)$$

where U_{Amax} = axial ion energy

L = length of the quadrupole rods

$$(10) \quad d_{max} = r_o \left(\frac{\Delta M}{M}\right)^{1/2}$$

where d_{max} = maximum allowable beam diameter for axially directed ions.

The power P required of the device is

$$(11) \quad P = 2.36 \times 10^{40} \text{ CM}^2 \nu^5 r_o^4 / Q$$

where C = total capacitance of the quadrupole

Q^* = figure of merit of the final tank circuit

of the r.f. generator.

B. Design Chart

1. Construction:

A design chart has been constructed to simplify the otherwise complicated interrelationships of quadrupole design parameters and thus to allow selection of characteristics that will be optimally matched to those of the cold cathode ion source.

For the detection of masses from 2 to 100 amu, selection of a mode where ΔM remains fixed and equal to 1 amu ensures that essentially no adjacent peak overlap will occur. Imposition of the

* No relation to the Q aperture plate symbol used elsewhere in the text.

requirements of equations (6) through (10) ensures essentially 100% transmission of stable ions. Design flexibility has thus been reduced. However, still unspecified and/or undetermined, are values for V , r_o , U_{Tmax} , d , P , U_{Amax} , L , γ and U .

To clarify the interdependency of these parameters, the preceding design equations have been rewritten in terms of a minimum number of variables. These are V , r_o , and L (While ΔM , M , C and Q also enter into the equations, they are fixed. ΔM is 1 amu, M has a maximum value of 100 amu and Q and C are made as high and low, respectively, as practicable; reasonable estimates of these values, which were used in the preceding equations are $Q=300$ and $C=100$ p.f.). Constants in the rewritten equations have been calculated for all variables in MKS units except for M and ΔM , which are in amu.

The following equations remain unchanged:

$$(8) \quad U_{Tmax} = \frac{V}{15} \left(\frac{\Delta M}{M} \right)$$

$$(9) \quad U_{Amax} = 5.82 \times 10^{-3} \frac{L^2 V}{r_o^2} \left(\frac{\Delta M}{M} \right)$$

$$(10) \quad d_{max} = r_o \left(\frac{\Delta M}{M} \right)^{1/2}$$

Equation (3) is rewritten to give γ explicitly in the new units

$$(3a) \quad \gamma = \frac{3710}{r_o} \sqrt{\frac{V}{M}}$$

Equation (11) is rewritten by substituting M from equation (3) and γ from equation (3a). This gives

$$(11a) \quad P = 1.52 \times 10^{-8} V^{5/2} / r_o M^{1/2}$$

Equation (5) is rewritten by substituting ν from (3a). This gives

$$(5a) \quad U = V(0.16784 - 0.125/M)$$

$$(5b) \quad U_{\max} \approx 0.168V \text{ (for } M=100 \text{ amu)}$$

The design chart was constructed from a selected range of values for V , r_o , and L using the above equations. It is shown in Figure 21.

V , r_o , and L are independent of each other. All other parameters depend on either V , r_o or both and are therefore tabulated to their right. L effects only U_{\max} and therefore heads only the U_{\max} columns. The chart is constructed with $M=100$ amu, the largest mass to be analyzed.

2. Interpretation and selection of values:

Once a design is chosen, r_o , L , ν , $U_{T\max}$, and $U_{A\max}$ remain fixed. L and r_o remain fixed because they pertain to the physical dimensions of the quadrupole (Figure 20). Frequency ν is kept fixed by mode choice. Fixed values of ν and r_o then force the ratio V/M to remain fixed (Equation 3a). Since $M=1$ amu, and since V/M , L and r_o are fixed, $U_{T\max}$ and $U_{A\max}$ must also remain fixed (Equations 8 and 9).

As a consequence of the above fixed values, V , d_{\max} , P and U are mass dependent. This is evident by inspection of Equations 3a, 10, 11a, and 5a, respectively. Since numerical chart values are calculated for $M=100$ amu, values of V , P and U shown are the maximum required, while d_{\max} is the smallest required.

V (volts)	r ₀ (cm)	U _{Tmax} (ev)	d _{max} (mm)	λ (MC)	P (watts)	U _{Amax} (ev)					U (volts)
						L=5cm	L=10cm	L=15cm	L=20cm	L=25cm	
500	0.500	0.330	0.500	1.66	1.70	2.89	11.6	25.9	46.4	72.6	84.0
	0.900	0.330	0.900	1.922	0.950	.893	3.56	8.00	14.2	22.4	84.0
	1.30	0.330	1.30	0.639	0.655	.428	1.71	3.84	6.85	10.7	84.0
	2.00	0.330	2.00	0.415	0.425	.181	.72	1.62	2.89	4.52	84.0
1000	0.50	0.670	0.50	2.34	9.60	5.75	23.0	51.8	92.1	144	167
	0.90	0.670	0.90	1.30	5.25	1.77	7.10	15.9	28.4	44.4	167
	1.30	0.670	1.30	0.900	3.69	.850	3.40	7.65	13.6	21.3	167
	2.00	0.670	2.00	0.585	2.40	.361	1.44	3.25	5.78	9.05	167
2000	0.50	1.34	0.50	3.32	54.5	11.6	46.2	104.0	185	299	334
	0.90	1.34	0.90	1.84	30.2	3.52	14.3	32.0	57.1	88.0	334
	1.30	1.34	1.30	1.28	21.0	1.73	6.90	15.5	24.2	43.1	334
	2.00	1.34	2.00	0.830	13.6	.725	2.90	6.6	11.6	18.4	334
3000	0.50	2.00	0.50	4.07	150	17.4	69.7	157	279	436	501
	0.90	2.00	0.90	2.26	83.0	5.38	21.4	48.6	85.6	129	501
	1.30	2.00	1.30	1.56	52.5	2.56	10.2	23.1	41.0	64.1	501
	2.00	2.00	2.00	1.03	38.0	1.11	4.45	10.0	17.8	27.9	501
7500	0.500	5.00	0.500	6.43	1480	43.6	174	392	697	1091	1250
	0.900	5.00	0.900	3.58	822	13.4	54.8	122	215	337	1250
	1.30	5.00	1.30	2.47	568	6.40	25.6	57.9	102	160	1250
	2.00	5.00	2.00	1.60	368	2.73	10.9	24.7	43.7	68.4	1250

FIG. 21 QUADRUPOLE MASS ANALYZER DESIGN CHART

Selection of the mutually independent parameters V (for mass 100), r_o and L specifies the quadrupole design. Determination of optimum values will now be considered.

It is evident from the chart that the larger V is made, the larger is the resulting analyzer sensitivity, since both U_{Tmax} and U_{Amax} are thereby increased. The value of V has no effect on the maximum allowable beam diameter d_{max} and it poses no design problem on frequency ν or steady state potential U over the ranges tabulated. The upper limit on V is determined by the associated power requirements P . The higher V is made the larger is the resulting P , with resultant increases in size and cost of the r.f. power supply. The Atlas quadrupole described by Brunnee⁽¹⁴⁾ uses a power supply whose size appears reasonable. It produces 30 watts of r.f. power, in addition to other power requirements. This is accomplished in a standard rack mounted chassis with 9 x 19 inches front panel dimensions. This would allow V in the 2000 to 3000 volt range and results in a U_{Tmax} of about 2.00 ev.

The chart illustrates that increasing r_o has two opposing effects on quadrupole sensitivity: (1) It increases the sensitivity by allowing increased beam diameter (Since d_{max} is proportional to r_o (Equation 10), area and hence sensitivity is proportional to r_o^2). (2) It decreases sensitivity by restricting the permissible axial ion energy. U_{Amax} is inversely proportional to r_o^2 (Equation 9). Experimental results indicate condition (1) to be overriding since the ion current rate of increase diminishes with increased ion

energy (Figure 10).

The chart also shows that increased r_0 results in a beneficial decrease in power requirements. Resultant frequency changes are unimportant and no other parameters are affected. The primary limitation on r_0 is the detrimental effect of large rod surface area on vacuum performance. (Rod radius is $1.16 \times r_0$. The diameter of the total cross sectional area of the instrument is $6.64 r_0$.) For V between 2000 and 3000 volts, an r_0 of about 1.0 cm appears to be a reasonable compromise.

It is obvious that L effects only U_{Amax} , which is proportional to L^2 (Equation 9). It is therefore desirable to make L as large as possible to increase sensitivity. However, the radial energy component limitations (about 2.00 ev) imposed by power requirement limitations, discussed above, limit the sensitivity gain resulting from very long rods; few ions can be anticipated to have less than a few percent of their total energy in a radial component. A U_{Amax} between 30 and 100 ev therefore appears adequate. This can be accomplished with a rod length of about 20 cm for the above selected values of r_0 and V .

SUMMARY AND CONCLUSIONS

A new experimental cold cathode ion source has been designed and constructed. The primary purpose was to investigate methods of increasing the source sensitivity obtained in the feasibility study, compatible with the requirements of a quadrupole mass spectrometer. The source contains a probe for measuring ion energy spectra through a 1 mm simulated quadrupole entrance aperture. The probe's position is adjustable relative to the ion exit aperture. The design includes an electrostatic lens and provision for comparing sensitivities both with and without the lens. Also included is provision for testing for optimum cathode potentials. Modifications have been made in the magnetic geometry used in the feasibility study source; cylindrical ceramic magnets have reduced external bulk considerably; elimination of pole pieces has increased accessibility to the ion exit aperture and reduced internal bulk and gas traps for improved UHV performance.

Methods of optimizing sensitivity without the lens were studied first. As a function of cathode potential, the sensitivity remained constant for positive values and rose appreciably (up to a factor of 7) for negative ones. An intense electron component accompanied the negative potentials however, making the higher sensitivities suspect; experiments conducted to verify them were judged inconclusive.

A family of ion energy spectra were obtained as a function of

distance from the ion exit aperture. The energy distributions over all distances and all cathode potentials (both positive and negative) showed ions predominating at low energies and decreasing continuously with increased energy, a situation beneficial to high quadrupole spectrometer sensitivity. Maximum sensitivity occurred nearest the exit aperture and again at a point more distant.

The highest sensitivity obtained for a positive pusher cathode potential (+40 volts for example) and an ion energy range of 0 to 30 ev (an acceptable energy range for a quadrupole spectrometer) was 5.5 ma/torr (nitrogen). This was recorded at both 0.14 inches and at 0.88 inches from the exit aperture. This sensitivity, obtained through the 1 mm diameter probe aperture compares with a somewhat lower figure obtained with a 3 mm diameter aperture used in the feasibility study. A minimum sensitivity improvement of 10 has therefore been achieved, without the use of a lens.

Frequent changes in sensitivity to pressure were observed in the magnetron portion of the source. Cathode current changes up to 35% were observed at constant pressure. Conditions to which this apparent operational mode switch is attributable, or the pressure region to which it is confined, were not investigated (due to leaking feedthroughs).

The sensitivity benefits of an electrostatic lens were next investigated. A three aperture einzel lens was designed for this

purpose. It has the advantage of focusing without increasing ion energy and enables suitable electronic coupling between source and quadrupole. Analytical investigations conducted to determine optimum design and operation revealed severe lens limitation for the particular conditions and requirements of the cold cathode ion source. It indicated that the lens would provide no benefit in increasing source sensitivity over placing the quadrupole close to the source, unless an especially favorable beam geometry existed (e.g. a nearly parallel and mono-energetic beam).

Experimental studies were conducted for several positions of lens and probe relative to the ion exit aperture. A large range of lens focusing potentials were applied and energy spectra were obtained for selected values. The effect of differing cathode potentials were also studied. It was concluded for each situation that the lens provided no sensitivity improvement. However, anomalies in lens operation were also observed. These were attributed to the presence of electrons in the beam and their resulting focusing and/or reflection. The results of electron reflection by the lens supported doubts about the validity of higher sensitivities obtained for negative cathode potentials.

A quadrupole mass analyzer design chart has been constructed covering a wide range of possible design values. Their interdependence, which is rather complicated is thereby made evident. As a result, a set of design parameters have been determined which are optimally matched to both the experimentally determined

characteristics of the cold cathode ion source and the objectives of a UHV mass spectrometer.

It is concluded that the next stage of development should involve the physical coupling of a quadrupole mass analyzer and the cold cathode ion source. The present basic source configuration should be used and situated so that the quadrupole entrance aperture is at one of the positions of greatest intensity. Both analysis and experimental results indicate that a lens will not benefit this situation.

BIBLIOGRAPHY

1. Redhead, P.A., The Magnetron Gauge: A Cold-Cathode Vacuum Gauge, Can. J. Phys., Vol. 37, pp. 1260-1271 (1959)
2. Hobson, J.P., and Redhead, P.A., Operation of an Inverted Magnetron Gauge in the Pressure Range 10^{-3} to 10^{-12} MM. Hg., Can. J. Phys., Vol. 36, pp. 271-288 (1958)
3. Torney, F.L., and Fowler, P., (National Research Corporation, 70 Memorial Drive, Cambridge, Mass.) Feasibility Study on the Design and Development of a Cold Cathode Ion Source, Final Report for Contract NAS1-2691, Task No. 2, (January 1964)
4. Hall, C.E., Introduction to Electron Microscopy, pp. 63-64, 184, McGraw-Hill, New York (1953)
5. Ibid., p. 51
6. Gabor, D., The Electron Microscope, p. 11, Chemical Publishing Company, New York (1948)
7. Hall, op. cit., p. 73
8. Zworykin, V.K., et al. Electron Optics and the Electron Microscope, p. 439, John Wiley and Sons, New York (1945)
9. Ibid., pp. 436-440
10. Hall, op. cit., p. 72
11. Zworykin, op. cit., p. 438
12. Klemperer, O., Electron Optics, pp. 4, 64, University Press, Cambridge, England (1953)

13. Helmer, J.C., and Jepson, R.L., Electrical Characteristics of a Penning Discharge, Proceedings of the I.R.E., 49, pp. 1920-1925, (1961)
14. Brunnee, C., et al. (Atlas Mess-Und Analysentechnik G.m.b.H., Bremen, Germany) presented at the Mass Spectrometry Conference, ASTM Committee E-14, May 1963, San Francisco, California